NATIONAL TECHNICAL UNIVERSITY OF ATHENS

SCHOOL OF CIVIL ENGINEERING

MSc in Analysis and Design of Earthquake Resistant Structures

Design and Optimization of Systems with Negative Stiffness Elements for Bridge Seismic Isolation

MSc Thesis

Syrimi Panagiota

Athens, February 2018

ΕΘΝΙΚΟ ΜΕΤΣΟΒΙΟ ΠΟΛΥΤΕΧΝΕΙΟ

ΣΧΟΛΗ ΠΟΛΙΤΙΚΩΝ ΜΗΧΑΝΙΚΩΝ

ΔΠΜΣ – Δομοστατικός Σχεδιασμός και Ανάλυση των Κατασκευών

Σχεδιασμός και Βελτιστοποιήση Συστημάτων Αρνητικής Στιβαρότητας για τη Σεισμική Μόνωση Γεφυρών

Μεταπτυχιακή Εργασία

Συρίμη Παναγιώτα

Αθήνα, Φεβρουάριος 2018

Στην οικογένειά μου

TABLE OF CONTENTS

Preface

This Master Thesis, entitled, "Design and Optimization of Systems with Negative Stiffness Elements for Bridge Seismic Isolation", aims to present possible implementation of a novel passive vibration absorption concept, the KDamper concept, to bridge structures. The main feature of KDamper devices is the incorporation of negative stiffness elements and the exploitation of their unique properties. As a result, the proposed mechanisms and configurations enlist as promising alternatives to conventional techniques for seismic effects mitigation.

In order to maintain its original purpose, the project consists of 6 chapters and 2 appendices, with the following structure: In Chapter 1, the basic principles of seismic isolation are presented. Useful definitions, descriptions and details on this contemporary seismic protection technique are given in this chapter, in view of providing basic background knowledge and information for a better understanding of the issues treated in the next chapters. In Chapter 2, the most commonly encountered contemporary bridge seismic isolation devices and methods are presented. A brief description of their specific characteristics and properties is given, along with the reasons that render them efficient and suitable (or not) for the mitigation of the effects of earthquake excitation on bridge structures. Chapter 3 includes a description of the main properties of negative stiffness elements. The employment of special mechanical configurations, in order to achieve the desired negative stiffness behavior, is also discussed, in view of combining them with the KDamper concept, introduced in Chapter 4. A description of the proposed device, incorporating negative stiffness elements, is given in this chapter, along with a detailed presentation of its main properties and features. The equations that control the performance of the KDamper are described, too. Chapter 5 contains the optimization process, on whose results the design of the KDamper is based. More precisely, the optimization algorithm, the design variables, their limits and the selected objective function are thoroughly presented. In Chapter 6, three different numerical applications, towards the implementation of the KDamper concept to bridge structures, are presented. The corresponding dynamic analysis results, validate not only the accuracy and effectiveness of the proposed seismic effects' mitigation method but, also, the robustness of the aforementioned optimization procedure. Finally, the two appendices contain information on

mathematical and algebraic manipulations, required throughout the design procedure and are considered to be useful to ensure the better understanding of the reader.

At this point, I feel obliged to thank Dr. Evangelos J. Sapountzakis, Professor NTUA, the supervisor of my Master Thesis, for assigning this project to me and for his constant support and consulting during this effort. Moreover, I would like to thank Professor Ioannis Antoniadis, from the School of Mechanical Engineering NTUA, for the valuable knowledge and experience he was willing to share regarding the KDamper concept, as well as Assistant Professor George Tsiatas, (University of Patras) for his precious help in the field of optimization. Last but not least, I would like to thank my family and, especially, my parents for their support and understanding throughout this project.

Panagiota Syrimi

Αντί προλόγου …

Σκοπός της παρούσας Μεταπτυχιακής Εργασίας, που τιτλοφορείται "Σχεδιασμός και Βελτιστοποίηση Συστημάτων Αρνητικής Στιβαρότητας για τη Σεισμική Μόνωση Γεφυρών" είναι η παρουσίαση δυνατών εφαρμογών σε γέφυρες, μίας καινοτόμας ιδέας για την απορρόφηση ταλαντώσεων, με την ονομασία KDamper. Το βασικό χαρακτηριστικό των συσκευών KDamper είναι η ενσωμάτωση στοιχείων αρνητικής στιβαρότητας και η αξιοποίηση των μοναδικών τους ιδιοτήτων. Ως αποτέλεσμα, οι προτεινόεμενς διατάξεις και μηχανισμοί αποτελούν αξιόλογες εναλλακτικές λύσεις στις συνήθεις πρακτικές για τη μείωση της επιρροής του σεισμού στις κατασκευές.

Προκειμένου να διατηρήσει τον πρωταρχικό της στόχο, η παρούσα εργασία αποτελείται από 6 κεφάλαια και 2 παραρτήματα που ακολουθούν την παρακάτω δομή: Στο Κεφάλαιο 1, παρουσιάζονται οι βασικές αρχές σεισμικής μόνωσης. Χρήσιμοι ορισμοί, περιγραφές και λεπτομέρειες πάνω σε αυτή τη σύγχρονη μέθοδο αντισεισμικής προστασίας δίνονται σε αυτό το κεφάλαιο, προκειμένου να προσφερθούν στον αναγώστη οι απαραίτητες πληροφορίες και το γνωστικό υπόβαθρο για την κατανόηση των θεμάτων που θα αναπτυχθούν στα επόμενα κεφάλαια. Στο Κεφάλαιο 2 παρουσιάνται οι πιο συχνά συναντώμενες συσκευές και μέθοδοι σεισμικής μόνωσης Μία σύντομη περιγραφή των ειδικών τους χαρακτηριστικών και ιδιοτήτων, δίνεται σε αυτό το κεφάλαιο μαζί με τους λόγους που τις καθιστούν αποτελεσματικές και κατάλληλες (ή το αντίθετο) για τη μείωση των επιρροών μιας σεισμικής διέγερσης σε μία γέφυρα. Το Κεφάλαιο 3 εμπεριέχει μία περιγραφή των βασικών ισιοτήτων των στοιχείων αρνητικής στιβαρότητας. Επιπλέον, αντικείμενο του κεφαλαίου αποτελεί και η εφαρμογή ειδικών μηχανολογικών διατάξεων προκειμένου να επιτευχθεί η επιθυμητή αρνητική στιβαρότητα και η αντίστοιχη συμπεριφορά στην κατασκευή. Οι διατάξεις αυτές είναι χρήσιμο να μελετηθούν συνδυαστικά και με το Κεφάλαιο 4, όπου η βασική ιδέα του KDamper παρουσιάζεται αναλυτικά, μαζί με τις ιδιότητες που το χαρακτηρίζουν αλλά και με τις διαφορικές εξισώσεις κίνησης που διέπουν τη δυναμική του συμπεριφορά. Το κεφάλαιο 5 περιλαμβάνεις τη διαδικασία βελτιστοποίησης στα αποτελέσματα της οποίας στηρίζεται ο σχεδιασμός συστημάτων με συσκευές KDamper. Πιο συγκεκριμένα, ο αλγόριθμός βελτιστοποίσης, οι μεταβλητές σχεδιασμού, τα όριά τους και η επιλεχθείσα αντικειμενική συνάρτηση παρουσιάζονται αναλυτικά. Στο Κεφάλαιο 6 παρουσιάζονται τρεις διαφορετικές αριθμητικές εφαρμογές του KDamper σε κατασκευές γεφυρών.

Τα αποτελέσματα των αντίστοιχων δυναμικών αναλύσεων πιστοποιούν όχι μόνο την και ακρίβεια και την αποτελεσματικότητα της προτεινόμενης μεθόδου μείωσης των επιρροών του σεισμού, αλλά και την ευστάθεια της προαναφερθείσας διαδικασίας βελτιστοποίησης. Κλείνοντας, τα δύο παραρτήματα περιέχουν πληροφορίες σχετικά με μαθηματικούς και αλγεβρικούς χειρισμού που διεξάγονται κατά τη διάρκεια της διαδικασίας σχεδιασμού και θεωρείται χρήσιμο για τη διασφάλιση της καλύτερης δυνατής κατανόησης από τον αναγνώστη.

Στο σημείο αυτό, οφείλω να ευχαριστήσω τον κ. Ευάγγελο Σαπουντζάκη, Καθηγητή ΕΜΠ, επιβλέποντα καθηγητή της Μεταπτυχιακής Εργασίας, για την ανάθεση του συγκεκριμένου θέματος αλλά και για τη συνεχή υποστήριξη και τις συμβουλές του καθ' όλη τη διάρκεια εκπόνησης της εργασίας. Επιπλέον, θα ήθελα να ευχαριστήσω τον κ. Ιωάννη Αντωνιάδη, Καθηγητή της Σχολή Μηχανολόγων Μηχανικών ΕΜΠ για τις γνώσεις και την εμπειρία του πάνω στο KDamper, τα οποία ήταν διατεθειμένος να μοιραστεί μαζί μας, αλλά και τον κ. Γεώργιο Τσιάτα, Αναπληρωτή Καθηγητή Πανεπιστημίου Πατρών για την πολύτιμη βοήθεια του στο κομμάτι της βελτιστοποίησης. Τέλος, θα ήθελα να ευχαριστήσω την οικογένειά μου και, ειδικά, τους γονείς μου για τη στήριξή και την κατανόησή τους κατά τη διάρκεια διεξαγωγής της παρούσας εργασίας.

Συρίμη Παναγιώτα

Abstract

In response to the damage generated by earthquakes occurring in densely populated areas, seismic design codes for the design of buildings, bridges and industrial facilities changed with the intention of leading to better seismic performance. Towards this direction, many strategies have been developed and proposed, with the idea of seismic isolation of structures being the most promising one. Focusing on bridge structures, numerous innovative devices and techniques have already been invented, tested and applied on real structures. Various types of bearings as well as more complex configurations, such as Tuned Mass Dampers (TMDs), enlist. Exploiting the positive features of TMDs and of devices with negative stiffness elements, while avoiding their negative ones, a novel passive vibration absorption and damping concept, the KDamper concept, is introduced, in view of mitigating the effects of seismic excitations on structures. A KDamper device contains both positive and negative stiffness elements, arranged in appropriate geometrical configurations. An additional mass, operating as an energy dissipating mechanism, similarly to TMDs, and an artificial damper are also required. A metaheuristic optimization algorithm, the Harmony Search (HS) algorithm is employed during the design procedure. Three different numerical applications, towards the implementation of the KDamper concept to bridge structures, are presented. The corresponding dynamic analysis results, validate not only the accuracy and effectiveness of the proposed seismic effects' mitigation method but, also, the robustness of the aforementioned optimization procedure.

Περίληψη

Στον αντίποδα των ζημιών που προκαλούνται από σεισμούς σε πυκνοκατοικημένες περιοχές, οι αντισεισμικοί κανονισμοί για το σχεδιασμό κτιριακών έργων, γεφυρών και βιομηχανικών εγκαταστάσεων αλλάζουν με την προοπτική να παρέχουν μία καλύτερη σεισμική απόδοση. Προς αυτήν την κατεύθυνση πολλέ στρατηγικές έχουν προταθεί και αναπτυχθεί κατά καιρούς, με τη σεισμική μόνωση να αποτελεί την καλύτερη δυνατή επιλογή. Ειδικά σε γέφυρες, πολυάριθμες καινοτόμες συσκευές έχουν ήδη εφευρεθεί, ελεχθεί πειραματικά και έχουν εφαρμοστεί σε πραγματικές κατασκευές. Διάφοροι τύποι εφεδράνων αλλά και πιο περίπλοκες διατάξεις, όπως οι Αποσβεστήρες Συντονισμένης Μάζας (TMDs) αποτελούν μερικά χαρακτηριστικά παραδείγματα. Αξιοποιώντας τις θετικές ιδιότητες των TMDs αλλά και των συσκευών που ενσωματώνουν στοχεία αρνητικής στιβαρότητας, αποφεύγοντας παράλληλα τα αρνητικά τους στοιχεία, εισάγεται μία καινοτόμα ιδέα για την παθητική απορρόφηση ταλαντώσεων με την ονομασία KDamper. Μία συσκευή KDamper αποτελείται τόσο από στοιχεία θετικής όσο και από στοιχεία αρνητικής στιβαρότητας τοποθετημένα σε κατάλληλες γεωμετρικές διατάξεις. Μία επιπλέον μάζα, που λειτουργεί ως μηχανισμός σκέδασης ενέργειας, και ένας τεχνητός αποσβεστήρας είναι επίσης απαραίτητοι. Ένας μεθευρετικός αλγόριθμος βελτιστοποίησης με την ονομασία the Harmony Search (HS) χρησιμοποιείται κατά τη διάρκεια της διαδικασίας σχεδιασμού. Τρεις διαφορετικές αριθμητικές εφαρμογές του KDamper σε κατασκευές γεφυρών παρουσιάζονται, ενώ τα αποτελέσματα των αντίστοιχων δυναμικών αναλύσεων πιστοποιούν όχι μόνο την ακρίβεια και την αποτελεσματικότητα της προτεινόμενης μεθόδου για τη μείωση των σεισμικών επιρροών στην κατασκευή, αλλά και την ευστάθεια της προαναφερθείσας διαδικασίας βελτιστοποίησης.

Chapter 1: Basic Principles of Seismic Isolation

In this chapter, the basic principles of seismic isolation are presented. Useful definitions, descriptions and details on this contemporary seismic protection technique are given hereby, in view of providing basic background knowledge and information for a better understanding of the issues treated in the next chapters.

1.1 INTRODUCTION

In response to the damage generated by earthquakes occurring in densely populated areas, seismic design codes for the design of buildings, bridges and industrial facilities changed with the intention of leading to better seismic performance. Towards this direction, many strategies have been developed and proposed, with the idea of seismic isolation of structures being the most promising one.

According to Kelly (1986) and Buckle and Mayes (1990), the main concept of seismic isolation, namely the decoupling of a structure from its base, leading to the mitigation of earthquake induced effects through energy absorption, is more than 100 years old. Since Calantarients (1909), who first proposed the separation of a building from its foundation by a layer of sand or talc, numerous approaches have been developed. Frank Lloyd Wright designed the Imperial Hotel in Tokyo in 1921, using a layer of soft mud, that lied underneath a layer of good soil, as a "cushion" to relieve the building from shocks (Wright 1977). Later on, the concept of the flexible first story was proposed by structural engineers (Martel 1929, Bednarski 1935, Green 1935, Jacobsen 1938). An improved version of this approach was introduced by Fintel and Khan (1969), with the assumption that the first-story columns yield during an earthquake. Even though this assumption offered the advantages of energy absorption and displacement control, the drastically reduced buckling load of the yielded columns leads the structure to instability and collapse.

Bearing systems made their appearance in the next decades, with roller bearings being the first ones (Ryuiti 1941, 1951, 1952, 1956, Caspe 1970, 1984). A demonstration building in Sebastopol, Crimea has been built on steel bearings (Nazin 1978). In the late 1970's, laminated natural rubber bearings with a cylindrical plug of lead in a central hole, namely the lead rubber bearings are developed in a government office building in Wellington (Robinson 1977). Since then, theoretical analysis of the response of structures with lead rubber bearings (Lee and Medland 1978, 1, 2, Lee 1980), as well as numerous shake table tests (Kelly and Hodder 1982) have been carried out. Lead rubber bearings still remain one of the most popular bearing system for seismic isolation. Sliding systems exploiting frictional restoring forces were the next to be introduced and analyzed (Ahmadi 1983, Mostaghel et al. 1982, 1983) due to their simple form and fail-safe action (Kelly and Beucke 1983). Finally, systems including helical springs and visco-dampers, commonly used in power plants to prevent the transmission of vibration from large components (e.g. turbine generators) into other parts of the structure, have been proposed for the seismic protection of full-size buildings (Tezcan and Civi 1979, Tezcan et al. 1980, Tezcan 1982, Huffman 1980). Further information on contemporary seismic isolation systems, especially on those applied to bridge structures, will be given in the next chapter of the current effort.

At this point, it should be mentioned that seismic isolation is a general concept suitable not only for new construction. On the contrary, it can be readily adapted to rehabilitation of older buildings of architectural and historic merit which presently do not comply with building codes.

1.2 BASIC PRINCIPLES

The main idea behind the concept of seismic isolation is to decrease the seismic forces induced into a structure during an earthquake, instead of increasing the structural capacity as in the conventional antiseismic techniques. This aim is accomplished through shifting (and specifically, increasing) the structure's eigenperiod, in view of the transition to the descending branch of the response spectrum of accelerations (Fig. 1.1a). The decoupling of the superstructure from the substructure or the implementation of devices incorporating negative stiffness elements enlist as examples of methods

allowing the value of structural eigenperiod to increase. When this period shift is significant it, simultaneously, results in an undesirable increase of displacements due to the different form and shape of the response spectrum of displacements (Fig. 1.1b). Even though the implication of dampers, to resolve this issue, seems a rather effective choice, it is not always a feasible one, as relatively high values of damping are usually required. An optimum compromise of the values of acceleration and displacement, within an acceptable range of the period, creates an area that provides potential solutions avoiding the negative effects described in the above. This area is called design window and its lower and upper bounds are depicted in Fig. 1.2.

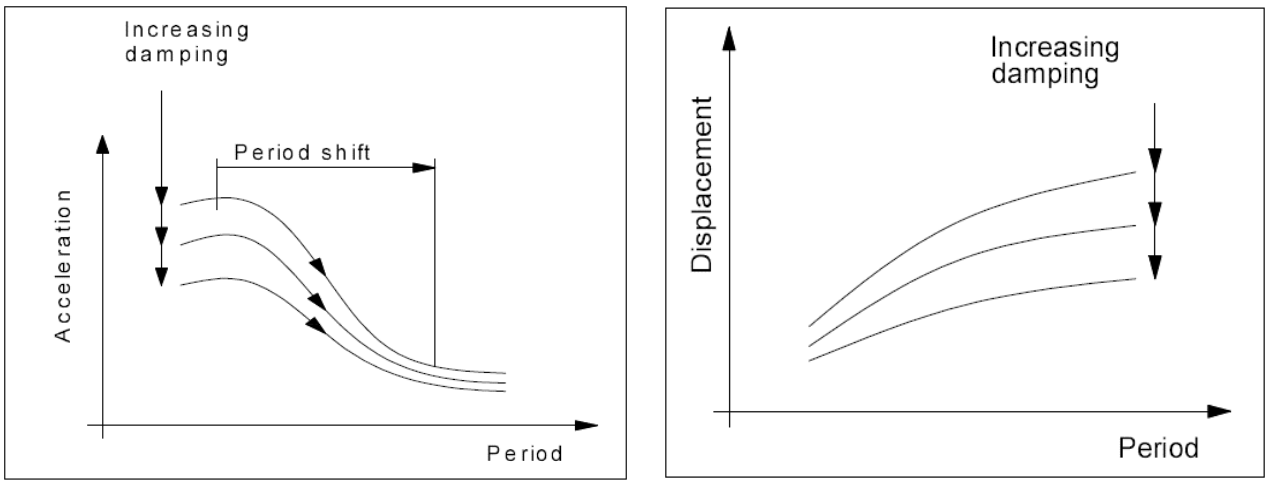

(a) (b)

Figure 1.1: Schematic representation of the response spectra in terms of (a) acceleration and (b) displacement.

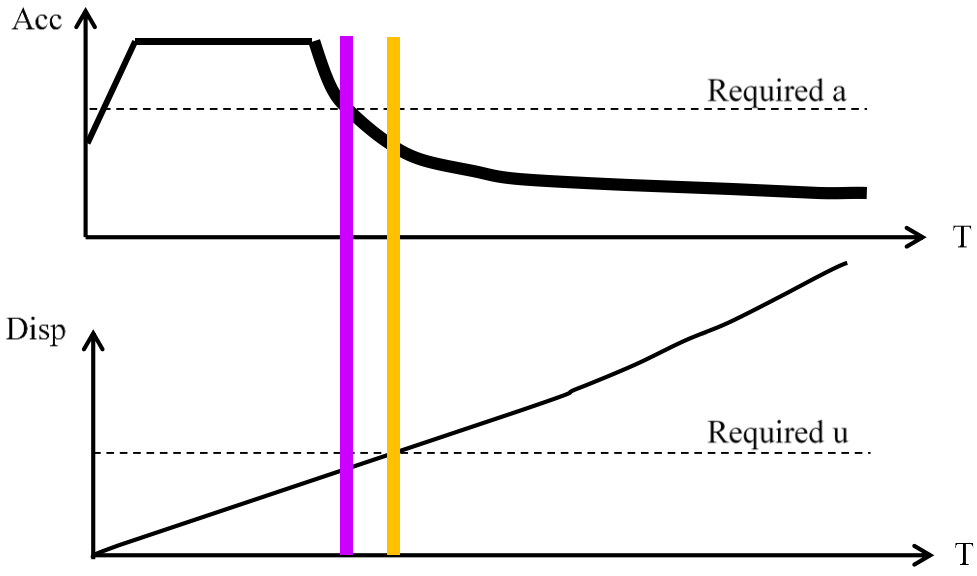

Figure 1.2: Conceptual illustration of the design window for seismic isolation systems.

At this point, it should be mentioned that the representation of response spectra in Figs. 1.1 is schematic, simulating, without disturbing generality, the curves provided in Eurocode 8. Corresponding response spectra in other regulations (e.g. American regulations) may follow different curves, however, their properties regarding the structure's eigenperiod, remain the same at any case.

Taking into account the conceptual illustration of Fig. 1.2, the criteria defining the boundaries of the aforementioned design window should be described. More specifically, the left boundary is imposed by the necessity to reduce seismic forces, satisfied through the reductions of accelerations. It, generally, depends on the site and soil conditions (the latter are responsible for the point of the design spectrum that separates the branch of constant accelerations from the descending one) and it is roughly estimated to be equal to 2 seconds. Concerning the right-side boundary, this cannot be defined as easily as the left one, as it is relevant to the displacement performance requirements of each structure. The upper limit of the design window, thus, depends on each structure's functionality, security and implementation demands. In light of the above, the need to introduce an optimization procedure for an efficient design of a seismic isolation system is inherently apparent. Further information on how this design window affects the design of seismic isolation systems and, especially, of the devices and configurations proposed in the following, can be found in Chapter 5 of this project.

Chapter 2:
Bridge Seismic Isolation Methods and Devices

In this chapter, the most commonly encountered contemporary bridge seismic isolation devices and methods are presented. A brief description of their specific characteristics and properties is given, along with the reasons that render them efficient and suitable (or not) for the mitigation of the effects of earthquake excitation on bridge structures.

2.1 INTRODUCTION

During the last decades, the most usual engineering approach, regarding the seismic protection of structures, is that, when a major earthquake event occurs, the safety of human lives is ensured, regardless the structural damages that may accompany it. Consequently, contemporary buildings are designed in view of satisfying at least failure criteria and/or collapse demands imposed by regulations. However, there are several types of structures, such as hospitals, dams and, of course, bridges, that are of special interest, since it is necessary to maintain their functionality not only during but, also, after a seismic event, in order to prevent any further fatal accidents. For this reason, many seismic isolation techniques are first applied in such structural systems, promising to offer an improved structural dynamic performance.

Focusing on bridge structures, numerous innovative devices and techniques have already been invented, tested and applied on real structures. The most commonly encountered among them are briefly described in the following sections of this chapter. Various types of bearings as well as more complex configurations, such as Tuned Mass Dampers, enlist.

2.2 TYPES OF BEARINGS

2.2.1 Simple elastomeric bearings

These are the simplest bearings that can be used as a form of seismic isolation of bridge structures. Nowadays, many bridges are supported on elastomeric bearings exploiting the advantages they offer over the conventional monolithic connection between the deck and the piers.

This type of bearings is, basically, made from natural (polyisoprene) or synthetic (polychloroprene-neoprene) rubber. Their stiffness in the vertical direction is slightly larger compared to that of the horizontal one. The rubber is considered to be undamped. In general, both kinds of rubber – either natural or synthetic – exhibit similar properties, for instance, their behavior depends on the temperature. However, the most commonly used kind is the natural rubber, since it demonstrates an overall enhanced performance under extreme shear deformations (larger value of deformation until rapture). Rubbers usually employed for seismic isolation contain carbon fillers that increase their strength over tearing, through increasing Young's modulus.

Rubber becomes stiffer under dynamic loading and its characteristics depend on temperature, range and frequency of the dynamic load. Moreover, rubber's properties are vulnerable to environmental factors, such as oxygen, radiation and ozone that many times are responsible for tearing on the surface of the rubber, accompanied by cracks and corrosion. To prevent the latter phenomena, antioxidants and anti-ozonous ingredients are introduced while manufacturing the bearing.

Finally, the use of such bearings on bridge structures requires frequent control and replacement to avoid failure.

2.2.2 Laminated bearings

Laminated bearings are an improved version of the simple elastomeric bearings. They consist of layers of rubber reinforced with thin layers of metal or fabric sheets, with metal sheets being the most common ones. The use of the above-mentioned elastic sheets limits the danger of lateral bulging, increasing by far the vertical stiffness of the bearing, without disturbing the horizontal one. A typical version of a laminated bearing is shown in Fig. 2.1.

When the bearing is compressed or rotated, lateral bulging appears due to the inability of rubber to compress. As a result, shear deformation is generated at the ends of the rubber layers. Typical types

of deformation of a laminated bearing under various types of loading are depicted in Fig. 2.2. Extreme levels of shear deformation at the ends of the rubber layers may damage the bearing or even lead to failure. The three loading conditions, included in Fig. 2.2, are not independent with each other. They coexist forming a load combination which subjects the bearings to compression, shear deformation and rotation at the same time. In general, small rotations may cause large shear deformations at the layers of rubber. Any potential additional tension on the rubber may lead to its failure. For this reason, some regulations do not allow the design of bearings under tension, aiming to preserve the wellbeing of the overall structure. Only a small amount of tension is allowed when the bearings lift.

Laminated bearings are categorized in two groups: (a) Low Damping Elastomeric Bearings – LEDBs and (b) High Damping Elastomeric Bearings – HDRBs.

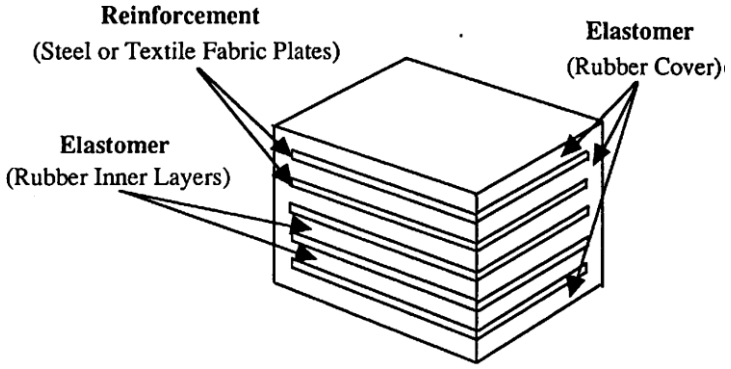

Figure 2.1: Laminated bearing.

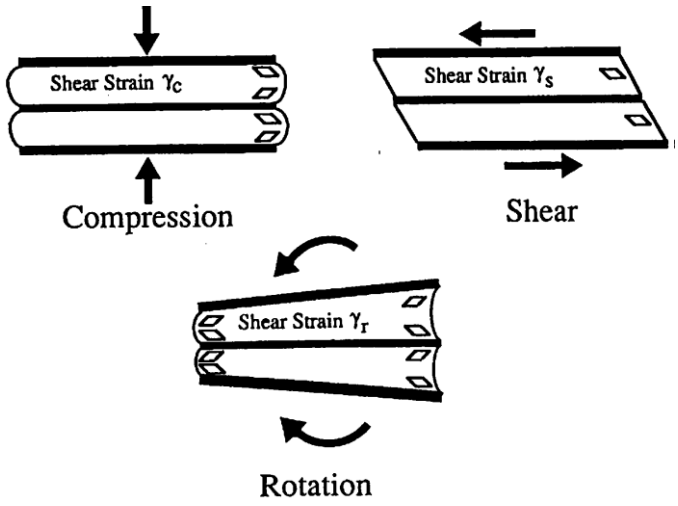

Figure 2.2: Tension and deformation of laminated bearings under different loading conditions.

(a) Low Damping Elastomeric Bearings – LEDBs

Low Damping Elastomeric Bearings (LEDBs), as depicted in Fig. 2.3, have found a wide range of applications in Japan, in combination with energy dissipation devices. This type of bearings consists of two metal plates of significant width at their top and bottom, along with many thinner metal sheets in the middle. As it has already been mentioned, the intermediate elastic sheets prohibit lateral bulging,

increasing vertical stiffness, without, simultaneously, disturbing the horizontal one. The latter is defined by the low shear modulus of the rubber. Their shear behavior is linear for an area of shear deformations around 100% with damping values about 2-3% of the critical.

LDEBs demonstrate numerous advantages as:

- They are easily manufactured.
- Their replacement cost is low enough to be acceptable after damaging from an earthquake event.
- They are easily simulated as linear springs when dynamic analyses are carried out.
- Their mechanical properties are not vulnerable to changes of temperature, the loading's time history or aging.

Their major disadvantage is the need for a complex complementary damping system to coexist.

In general, LDEBs are considered to be an acceptable solution in antiseismic design of bridge structures only in areas with low seismic demands.

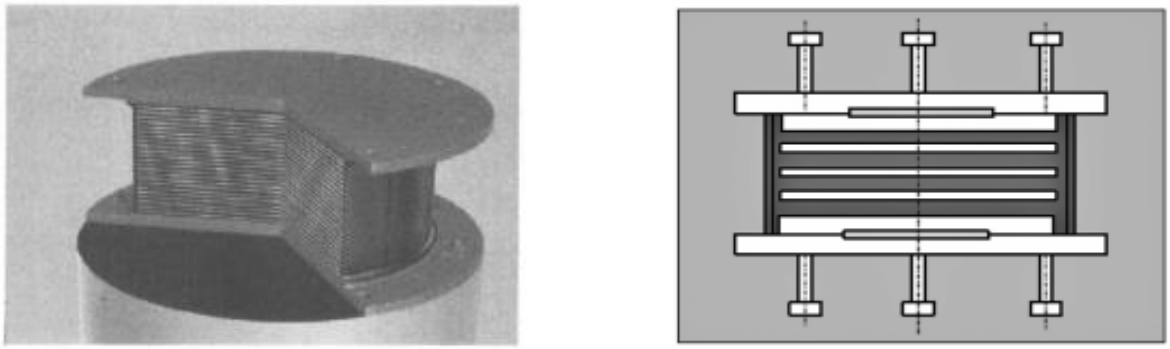

Figure 2.3: Low damping elastomeric bearings - LDEBs.

(b) High Damping Elastomeric Bearings – HEDBs

High Damping Elastomeric Bearings (HEDBs), as depicted in Fig. 2.4, is based on the recently accomplished development of the rubber containing inherent damping, without the necessity for additional energy dissipation devices. The damping od the bearings increases due to the introduction of extremely thin fragments of carbon, special oils or resins into the rubber. The ingredient of the fragments depends on the construction company. In general, they comprise of thinner layers of rubber compared to LEDBs, in order to be stiffer in the vertical direction, since the rubber used is of lower strength because of the additional fragments.

The maximum value of shear deformation ranges between 200% and 350%, while damping values higher than 5%, e.g. 10-20% may be obtained for a shear de3formation of 100%. Their effective stiffness and damping depends on the rubber quality and its components, the vertical axial compressing load, the loading velocity, the time history of the loading and the temperature. Their damping is neither viscous nor hysteretic but something in the middle. Thus, the HDEBs' damping is simulated as a linear combination of viscoelastic and elastoplastic behavior.

Finally, another important advantage of this type of bearings is that they significantly reduce structural vibrations. The bearings operate as filters not allowing high frequency vertical vibrations, due to traffic loads or adjacent underground railways, to develop.

Figure 2.4: High damping elastomeric bearings - HDEBs.

2.2.3 Lead-Rubber Bearings - LRBs

Lead-Rubber Bearings (LRBs) are reinforced rubber bearings similar to LDEBs. The only difference between them is that LRBs contain a single or multiple lead cores, placed inside the bearing through holes, as shown in Figs. 2.5 and 2.6. The thin horizontal metal sheets subject the core to shear deformation under horizontal dynamic loads and guarantee core restriction along with vertical stiffness and high levels of vertical capacity. Since their first appearance in 1970, LRBs have been vastly used in New Zealand, Japan and the United States. LRBs with more than one lead cores are not very common, while available information on their mechanical properties is limited.

The lead core offers energy dissipation whose magnitude depends on its diameter and its height. These bearings are quite stiff in the vertical direction but flexible in the horizontal one when the lead core yields.

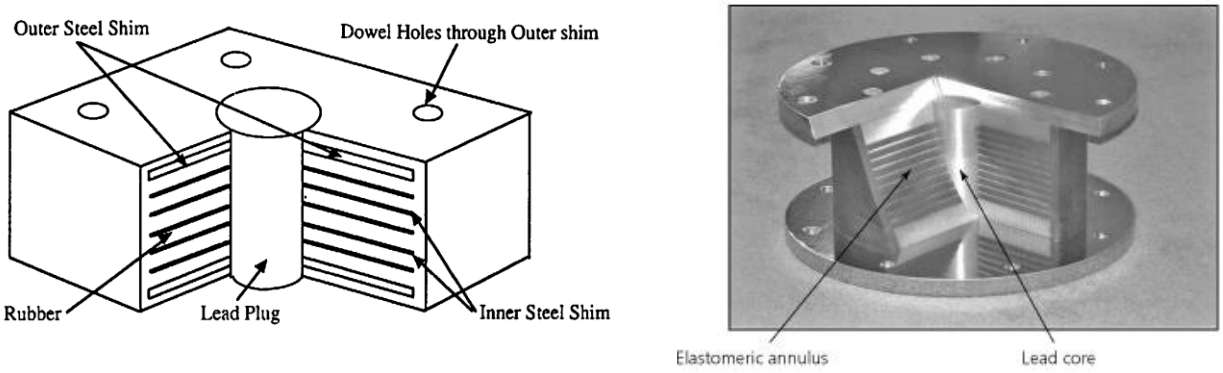

Figure 2.5: Lead-rubber bearings - LRBs.

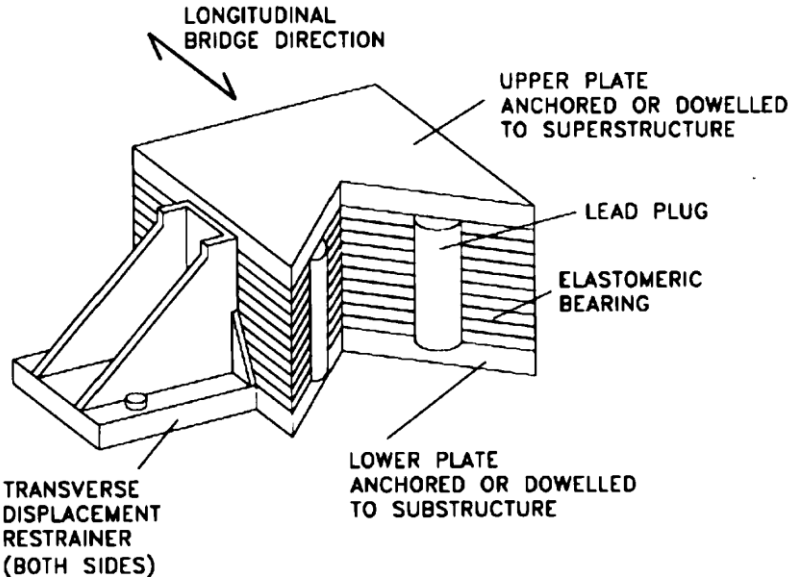

Figure 2.6: LRB with multiple lead cores (used in Japan).

The basic advantages of LRBs for the seismic isolation of bridge structures are their trustworthy behavior, the high damping values that are offered to the structure and the simplicity with which they are initial placed and replaced.

LRBs' horizontal force – horizontal displacement path is depicted in Fig. 2.7. Finally, it should be noticed that circular bearings are preferred over rectangular ones, since their properties remain the same at all spatial directions.

2.2.4 Sliding Bearings

(a) Flat Sliding Bearings

Flat sliding bearing limit the force transferred to the superstructure.

The dynamic friction factor depends, mainly, on the composition of sliding surfaces, the use of grease or not, the pressure on the sliding surface, and the velocity of sliding. Proper tests are suggested for its determination. Practically, values of the dynamic friction factor between 0.10 and 0.15 have been recorded during seismic events. When the ratio of the horizontal force over the vertical one is lower than the friction factor, the system behaves linearly. When the aforementioned ratio surpasses the friction factor, sliding develops and the value of shear force keeps rising. This way, a significant reduction of seismic forces is achieved, accompanied by large remaining deformations. Consequently, once this type of bearings is employed for the seismic isolation of a bridge, a means to reinstate the structure to its initial position is necessary. For this reason, flat sliding bearings are often combined with elastomeric bearings that offer the desired reinstatement.

(i) Pot Bearings

Their fundamental function is based on the fact that a cylindrical elastomeric disk is incorporated into a metal container, which is covered by a piston, transferring vertical compressive loads to the rubber. Thus, the rubber is compressed without the ability to change volume and, by extent, it resists significantly large compressive loads and undertakes rotations imposed by the structure.

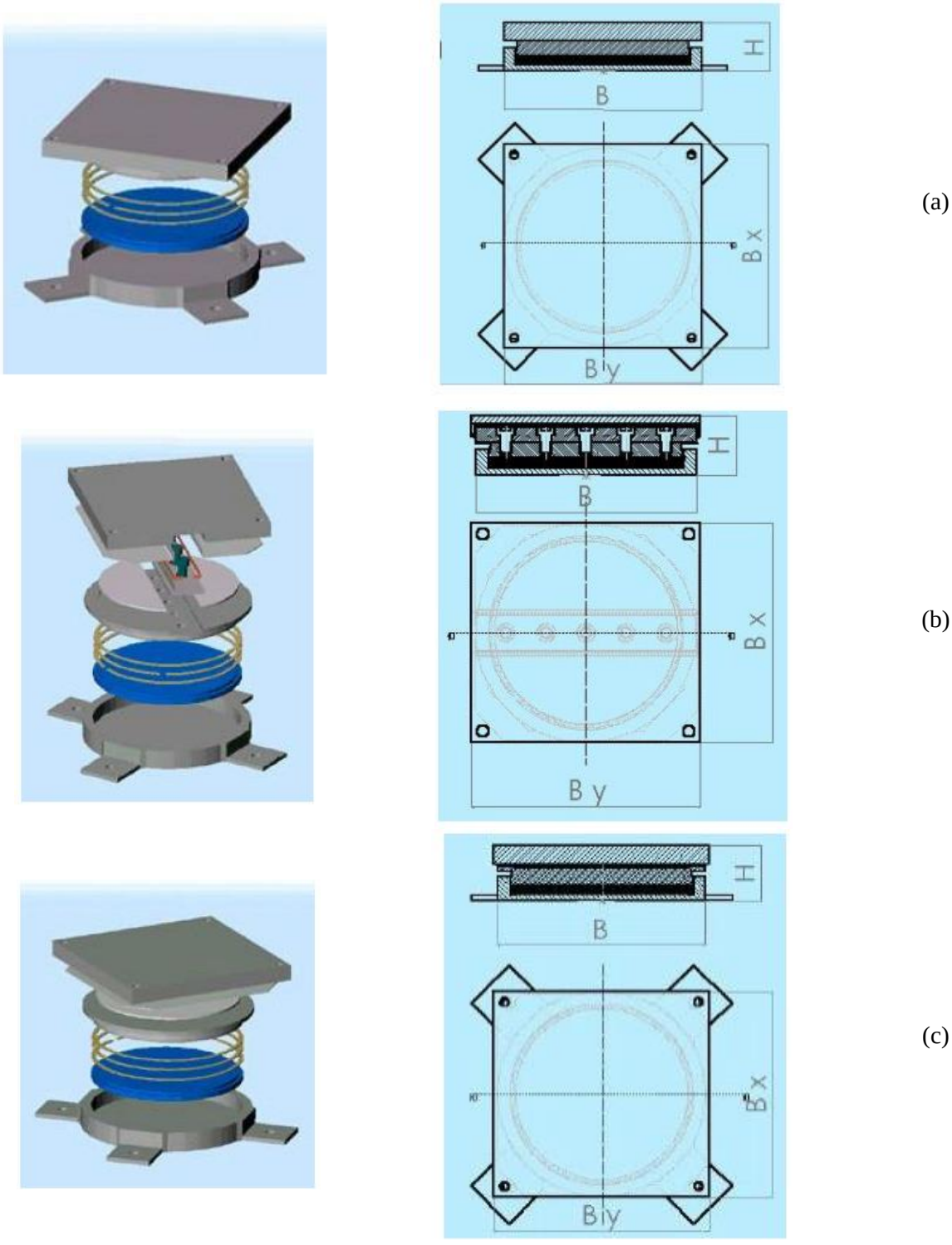

Figure 2.7: Different categories of pot bearings.

Depending on their construction, they may or may not allow horizontal displacements. Pot bearings are categorized in the following groups:

- Fixed pot bearings: they allow rotation about any direction, whereas the structure is restrained horizontally (Fig. 2.7a).
- Pot bearings allowing displacements in one horizontal direction (Fig. 2.7b).

- Pot bearings allowing displacements in multiple horizontal directions (Fig. 2.7c).

The positive features of pot bearings are the following:

- High vertical capacity levels with a small contact surface.
- The vertical loads are uniformly dispersed through the bearing due to the hydrostatic pressure of the incorporated rubber.
- The produced elastic forces are smaller than the ones of other types of bearings.
- They provide the structure satisfactorily ensuring functionality.

On the negative side:

- Pot bearings exhibit limited rotational abilities, which, however, is satisfying for most structures.
- Their placement requires more accuracy than bridge structures require.
- Their construction demands advanced technology, strict regulations, quality tests and more accuracy (little manufacturing tolerances).
- Their cost is higher compared to the one of elastomeric bearings.
- Except for the bearing's metal elements which are in contact with each other and the internal wall of the metal container, the rest of the metal parts need to be protected against corrosion.

(ii) *Disk, Ball and Socket and Eradiquake (USA) Bearings*

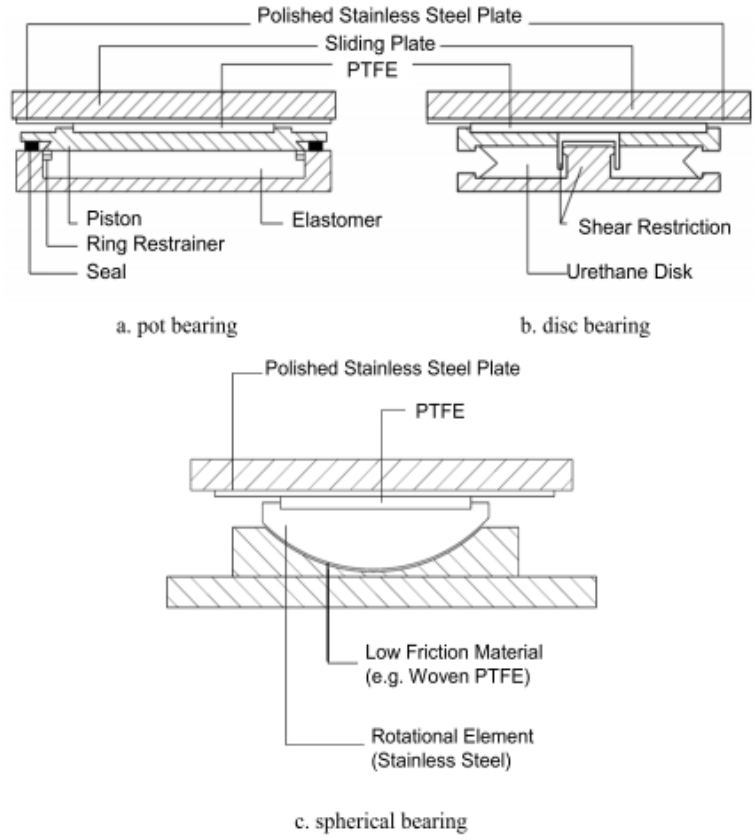

Figure 2.8: (a) Pot bearing, (b) disc bearing and (c) spherical bearing.

These types of bearings, as depicted in Fig. 2.8, are mostly used in the USA. They are included here for completeness reasons.

Eradiquake bearings (Fig. 2.9), are the only ones that differ, since they comprise of a system of orthogonally aligned polyurethane springs which act as force resetting elements.

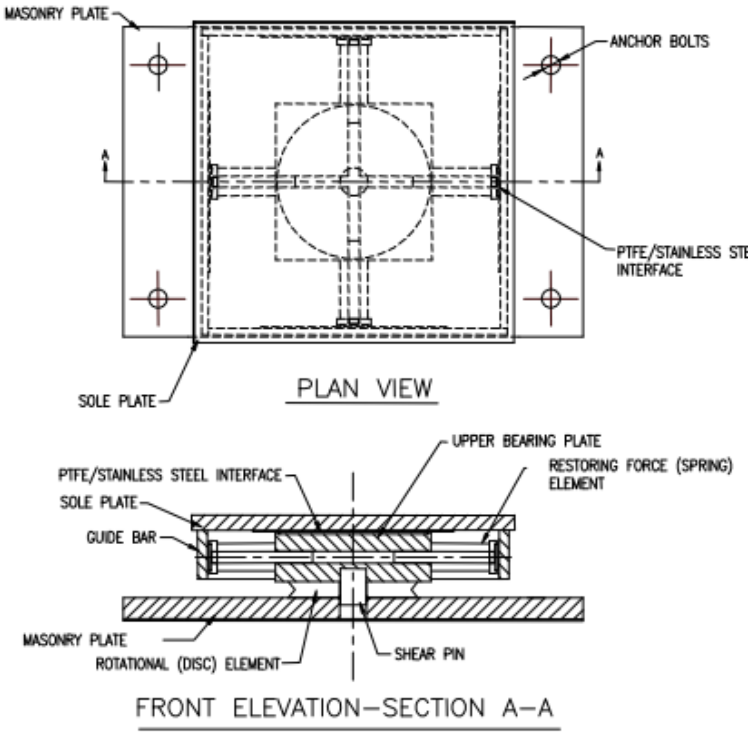

Figure 2.9: Eradiquake bearing

(b) Spherical Sliding Bearings – Friction Pendulum Systems

(i) FPS Bearings with one spherical sliding surface

In this type of bearings, sliding takes place on a curved surface, providing the structure with reinstating capabilities, due to the bearing's geometry after the end of the seismic event. The horizontal stiffness of such bearings depends on their weight, whereas their eigenperiod is independent from the mass (pendulum function).

More precisely, these bearings (Fig. 2.10) comprise of an almost hemispherical metal articulated slider that moves on a spherical stainless-steel surface. The friction factor on that surface is low, around 0.05-0.10 and may further decrease with the use of grease. The part of the slider that is in contact with the spherical surface, namely the concave surface, is covered with low friction composite liner material (PTFE). The other side of the slider is covered with Teflon and lies on a spherical cavity and has the ability to rotate inside it. As the slider moves on the spherical surface, it causes the superstructure (for instance the deck of a bridge) to rise. The latter, due to its own weight, provides the system with a reinstating force. Thus, the system returns to its equilibrium position.

Moreover, the friction developed between the slider and the spherical surface produces damping, while the bearings move. The effective stiffness of such bearings and the vibrating eigenperiod of the isolation system are defined by the curvature of the spherical sliding surface. The eigenperiod is

proportionate to the curvature radius and, consequently, the larger the curvature radius the higher the eigenperiod.

The combination of low values of friction along with the reinstating force, provided by the spherical sliding surface, results in an approximately bilinear hysteretic behavior, with an inherent capability of the system to regain its equilibrium.

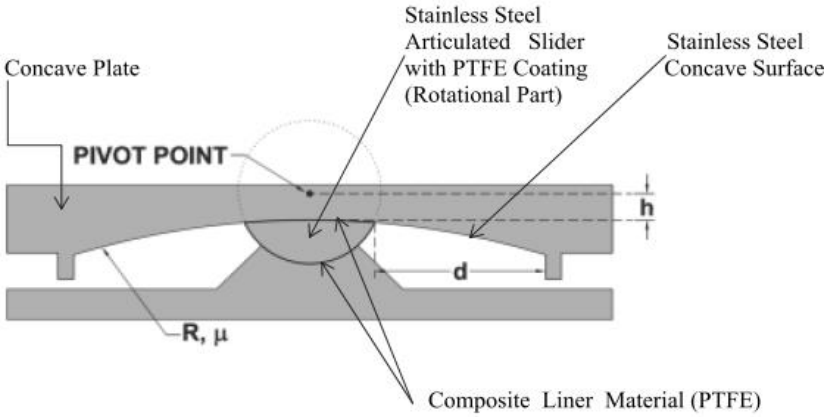

Figure 2.10: FPS with one spherical sliding surface.

(ii) <u>FPS Bearings with two spherical sliding surfaces</u>

This type of bearings consists of two external concave plates within which an almost spherical metal item, on which another concave metal item is adjusted, slides (Fig. 2.11). Practically, there are two sliders that move not only on the upper and lower spherical surfaces, but, also, with each other.

Their behavior is similar to the one of FPS bearings with one spherical sliding surface. Employing them on seismic isolation systems does not offer any extra advantages or improvements, compared to the bearings with one spherical surface. On the contrary, it complicates analyses. For these reasons, they are not commonly used.

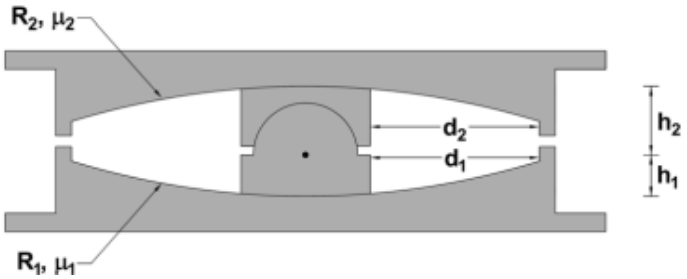

Figure 2.11: FPS with two spherical sliding surfaces.

(iii) <u>FPS Bearings with three spherical sliding surfaces</u>

The behavior of these bearings is more complex than the previous ones. A schematic representation of this type of bearings is given in Fig. 2.12, whereas a detailed analysis regarding their performance can be found in Constantinou et al. (2011).

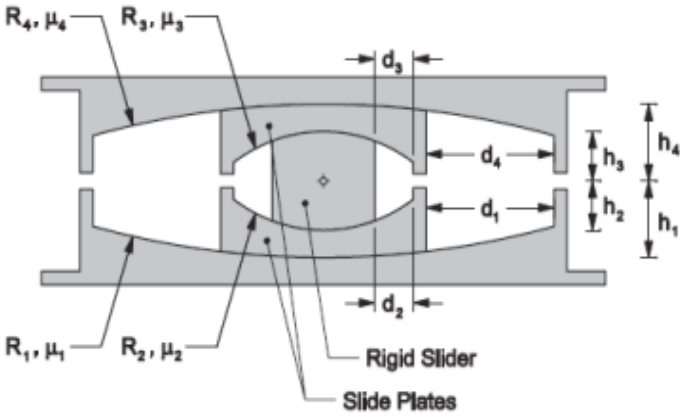

Figure 2.12: FPS with three spherical sliding surfaces.

2.2.5 Special Type Bearings

(a) Rocker Bearings

Rocker bearings consist of a curved spherical surface that rolls over a flat or concave spherical surface of bigger radius, as depicted in Fig. 2.13. It is suggested that the surfaces in contact should be of equal strength and hardness. Furthermore, the surfaces in contact should not be able to slide with each other. The fundamental function of these bearings is based on the absorption of displacements due to expansion and contraction.

The basic parts of rocker bearings are:

- Rocker: metal item with a curved surface on the one side. The curve may be cylindrical or spherical.
- Rocker plate: metal item in contact with rocker. The side that is in contact with the rocker may be flat or spherical.
- Shear dowels: they provide mechanical resistance against horizontal loads.

Such bearings are capable of transferring not only vertical but, also, horizontal forces from the superstructure to the substructure. They are categorized in two groups:

- Line rockers: they allow rotation only regarding one direction and, specifically, around the axis that is parallel to the line of contact. Their curved surfaces should be cylindrical.
- Point rockers: they allow rotation around any axis. Their curved surfaces should be spherical.

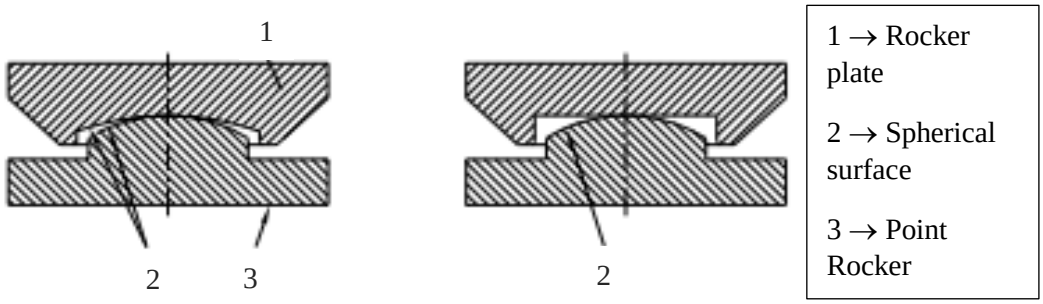

Figure 2.13: Rocker bearings.

The range of rotation depends on the geometry and the manufacturer and its maximum value is equal to 0.05 rad. The material used to create them is carbon, cast or stainless steel and cast iron. Under

normal conditions, the moments and horizontal forces occurring from the movement of such bearings are small and insignificant. However, due to the fact that their basic ingredient is steel, rocker bearings are susceptible to corrosion phenomena. A corroded bearing will induce larger forces and, as a result, constant monitoring and maintenance are absolutely necessary.

Rocker bearings, as well as roller bearings, described in the following, are not suggested for application on antiseismic bridge design and seismic isolation techniques.

(b) Roller Bearings

Roller bearings, as depicted in Fig. 2.14, comprise of one or more cylinders placed between two plates, the top and the bottom one. If there is only one cylinder, the bearing undergoes rotation around the contact line of the cylinder with the metal plates and horizontal displacements in the longitudinal direction. A bearing with more than one cylinders undergoes only horizontal displacements. If this is the case, a rocker bearing may be combined with the roller one, as shown at case 8 of Fig. 2.14. Roller bearings with only one cylinder may transfer small vertical axial compressing loads, but they are very economic to manufacture. Roller bearings with multiple cylinders exhibit exactly the opposite behavior.

The range of rotation depends on the geometry and the manufacturer and its maximum value is equal to 0.05 rad. The material used to create them is carbon, cast or stainless steel. The surfaces in contact should be of equal strength and hardness. Roller bearings present the same problems regarding corrosion, just like rocker bearings.

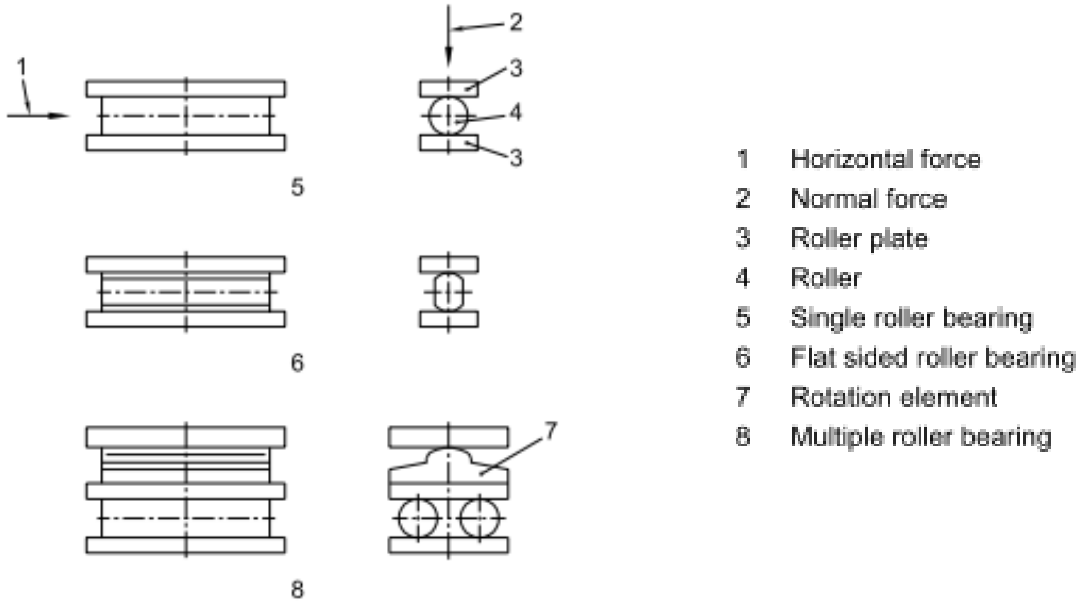

Figure 2.14: Roller bearings.

2.3 TUNED MASS DAMPERS (TMDs)

A Tuned Mass Damper (TMD), sometimes referred to as a dynamic vibration absorber, is a classical engineering device consisting of a mass, a spring and a viscous damper (Fig. 2.15). The TMD concept was first applied by Frahm (1909). Since Den Hartog (1956) first proposed an optimal design theory for the TMD for an undamped SDoF structure, the TMD has been employed on a vast array of

systems with skyscrapers being among the most interesting ones (Luft, 1977), (McNamara, 1979), (Qin et al., 2009). A characteristic example of its implementation on skyscrapers can be found in one of the tallest buildings in the world (Fig. 2.16), Taipei 101 Tower (101 stories, 504 m) in Taiwan (Haskett et al., 2003). Recent studies also include the use of TMDs for vibration absorption in seismic or other forms of excitation of bridge structures (Debnath et al., 2015). The natural frequency of the TMD is tuned in resonance with the fundamental mode of the primary structure. Thus, a large amount of the structural vibrating energy is transferred to the TMD and then dissipated through damping. Even though TMDs are known for their effectiveness and their reliability, the main disadvantage of such devices is the sensitivity of their properties. Environmental influences and other external parameters may alter the TMD properties, disturbing its tuning. Consequently, the device's performance can be significantly reduced (Weber and Feltrin, 2010). Another essential limitation of the TMD is that a large oscillating mass is required in order to achieve significant vibration reduction rendering its construction and placement procedure rather difficult.

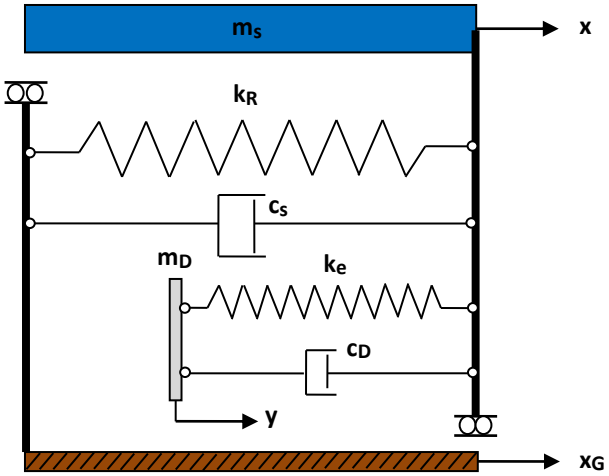

Figure 2.15: Schematic representation of a Tuned Mass Damper (TMD).

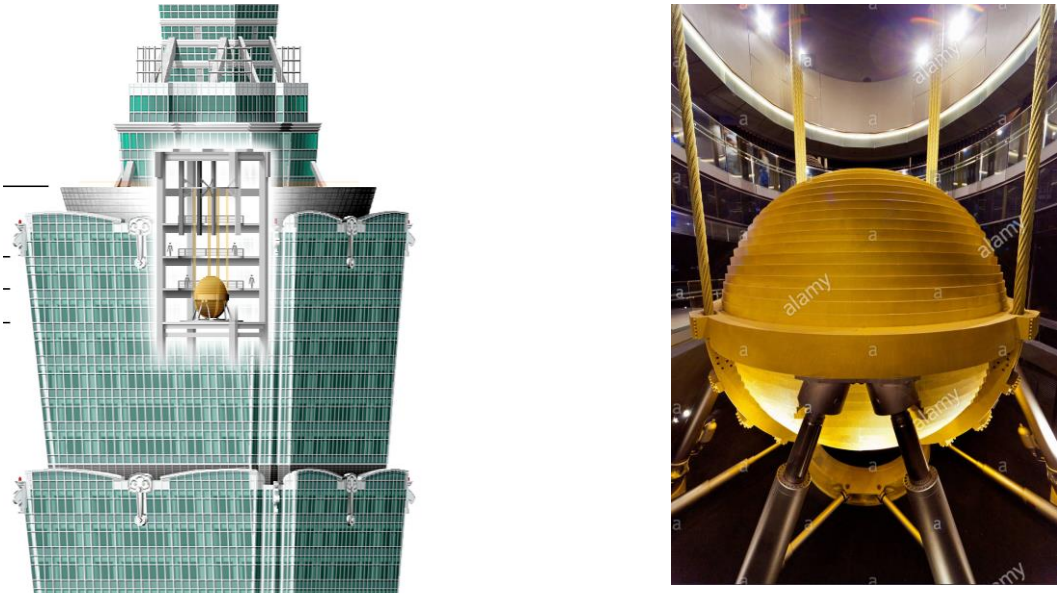

Figure 2.16: TMD on the Taipei 101 Tower in Taiwan.

Chapter 3:
Negative Stiffness Elements

In this chapter, a description of the main properties of negative stiffness elements is presented. The employment of special mechanical configurations, in order to achieve the desired negative stiffness behavior, is also discussed in the following, in view of combining them with the KDamper concept (Chapter 4).

3.1 INTRODUCTION

True negative stiffness is defined as a force that assists motion, instead of opposing it as in conventional positive stiffness elements (Fig. 3.1).

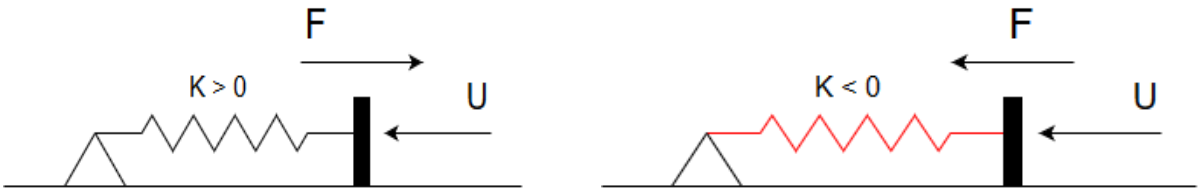

(a) (b)

Figure 3.1: Schematic representation of (a) a positive stiffness element and (b) a negative stiffness element.

The use of negative stiffness elements (or "anti-springs) for vibration isolation was first introduced in the pioneering publication of Molyneaux (1957), as well as in the milestone developments of Platus (1992). The central concept of these approaches is the significant reduction of the isolator's stiffness, which, consequently, leads to the decrease of the natural frequency of the system (the system's eigenperiod is increased) even at almost zero levels, as in Carella et al. (2007), being, thus, called "Quasi-Zero Stiffness" (QZS) oscillators. This way, enhanced vibration absorption is achieved, since the system exhibits reduced transmissibility for all operating frequencies above the natural one. Through numerical simulations and experimental testing, numerous researchers have demonstrated the effectiveness of this kind of devices. An initial comprehensive review of such designs can be found in Ibrahim (2008). Nagarajaiah et al. (2010) introduced a new structural modification approach for the seismic protection of structures using an adaptive negative stiffness device that resulted in the decrease of the dynamic forces imposed on the structure. The simultaneous growth of structural displacements, was prohibited by a damper, placed in parallel with the negative stiffness device.

The negative stiffness behavior is primarily achieved by special mechanical designs involving conventional positive stiffness pre-stressed elastic mechanical elements, such as post-buckled beams, plates, shells and pre-compressed springs, arranged in appropriate geometrical configurations. Some interesting designs are described in Winterflood et al. (2002) and Virgin et al. (2008). Alternatively, to elastic forces, other forms of physical forces can be employed to produce an equivalent negative stiffness effect, namely gravitational forces (Dyskin and Pasternak, 2012), magnetic forces (Robertson et al., 2009) or electromagnetic ones (Zhou and Liu, 2010). However, when dealing with seismic effects mitigation on buildings or bridge structures, where the values of negative stiffness required are quite high, elastic forces seem to be the only feasible choice.

Among others, QZS oscillators find numerous applications in seismic isolation (DeSalvo, 2007), (Iemura and Pradono, 2009), (Sarlis et al., 2011), (Attary et al., 2012a), (Attary et al., 2012b), (Pasala et al., 2012), (Sarlis et al., 2012), (Attary et al., 2015), in all types of automotive suspensions (Lee et al., 2007), (Le and Ahn, 2011), (Lee and Goverdovskiy, 2012), in torsional vibrations (Zhou et al., 2015) or in materials comprising of a negative stiffness phase (Lakes, 2001), not only at a material level (Taglinski, 2007), but, also, at macroscopic devices (Dong and Lakes, 2013). Quite recently, periodic cellular structures with advanced dynamic behavior have been also proposed, combining high

positive and negative stiffness (Michelis and Spitas, 2010), (Baravelli and Ruzzene, 2013), (Virk et al., 2013), (Correa et al., 2015).

However, QZS oscillators suffer from their fundamental requirement for a drastic reduction of the total structural stiffness almost to negligible levels, which limits the static load capacity of such structures.

In this effort, the positive features of the negative stiffness elements are combined with the advantages of the TMDs in order to design a novel passive vibration absorption concept, the KDamper concept, that overcomes the drawbacks of the two aforementioned techniques. A detailed description of the proposed concept is provided in Chapter 4.

In the next sections of the current chapter, the properties and the behavior of special configurations producing the desired negative stiffness effect is discussed. Precisely, the mechanism involved in the QZS oscillator of Carella et al. (2007) is presented hereby, along with two alternative proposed configurations, suitable for structural seismic protection applications.

3.2 "QUASI-ZERO STIFFNESS" CONFIGURATION

In Fig. 3.2a, one of the simplest configurations exhibiting quasi-zero stiffness behavior is depicted, proposed by Carella et al. (2007), comprising of a combination of positive and negative stiffness elements.

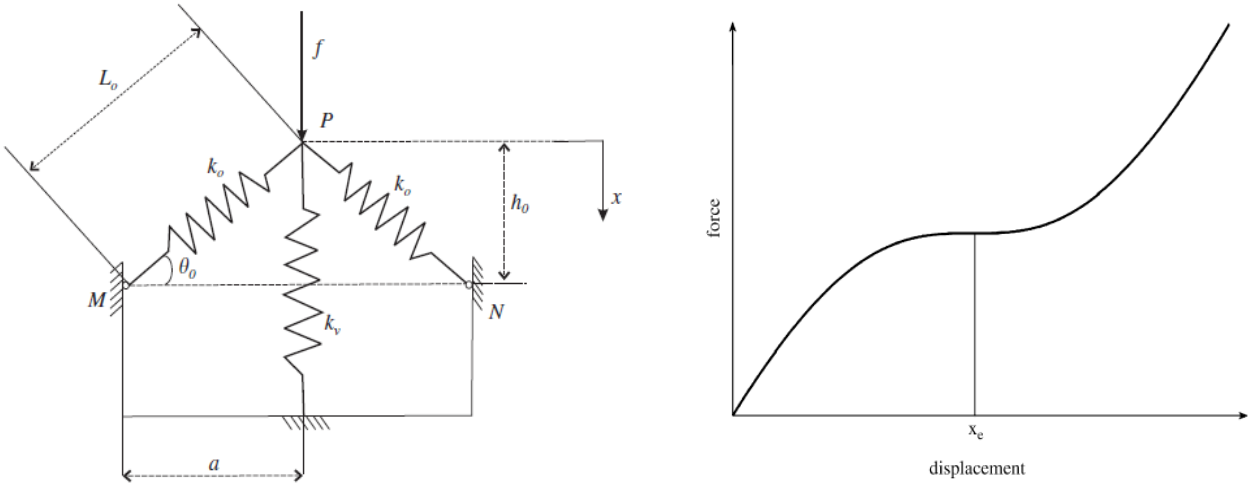

(a) (b)

Figure 3.2: (a) Schematic representation of the simplest system which can exhibit quasi-zero stiffness. (b) Typical force-displacement characteristic of the system. (Carella et al., 2007)

While the force, f is augmenting, for instance, due to loading with a suitably sized mass, the springs compress such that the oblique springs, k_o become horizontal and the static load is undertaken by the vertical spring, k_v. This state is the static equilibrium position of the system. Considering any movement about this equilibrium position, the positive stiffness of the vertical spring is counteracted by the oblique springs, which act as a negative stiffness element in the vertical direction. A typical

force-displacement curve for this system is given in Fig. 3.2b. In this diagram, x_e denotes the static equilibrium position and for this case, the system is designed such that the dynamic stiffness at this point is equal to zero. However, the penalty for this choice is that for large excursions from the equilibrium position, the system becomes stiffer than the vertical spring alone.

For the configuration of Fig. 3.2a, the non-dimensional stiffness, $\hat{K}_{QZS}$ along with the geometric dimension, a, aiming to achieve the desired QZS effect are calculated according to Eqs. (3.2.1)

$$\hat{K}_{QZS} = 1 + \frac{\gamma_{QZS}}{1-\gamma_{QZS}} \left[1 - \frac{\gamma_{QZS}^2}{\left(\hat{x}^2 - 2\sqrt{1-\gamma_{QZS}^2}\,\hat{x} + 1 \right)^{3/2}} \right] \tag{3.2.1a}$$

$$a = \frac{\gamma_{QZS}}{2\left(1-\gamma_{QZS}\right)} \tag{3.2.1b}$$

where $\hat{x}$ is the non-dimensional displacement of the system from its equilibrium position and γ_{QZS} is a geometrical parameter. After the solution of a suitable optimization problem regarding the range of displacements for which the system's non-dimensional stiffness, $\hat{K}_{QZS}$ remains lower than a prescribed value $\hat{K}_o$, namely, $\hat{K}_{QZS} < \hat{K}_o$, the optimal value of $\gamma_{QZS} = \gamma_{opt}$ is given from Eq. (3.2.2)

$$\gamma_{opt} \approx \left(\frac{2}{3} \right)^{\left(\hat{K}_o/2\right)+1} \tag{3.2.2}$$

It should be noted here that, since all aforementioned parameters are non-dimensional with regard to the vertical spring's stiffness, k_v and the oblique springs' length, L_o, $\hat{K}_o = 1$ means that the system's stiffness is equal to that of the vertical spring. For a thorough description of the mechanism's function and properties and an analytical presentation of its optimal design readers are referenced to Carella et al., (2007).

3.3 ALTERNATIVE PROPOSED CONFIGURATIONS

3.3.1 Proposed Configuration 1 – Pre-compressed springs

Regarding the properties and features of the simple QZS configuration proposed by Carella et al. (2007), an alternative mechanism is hereby described, as depicted in Fig. 3.3. Precisely, the static equilibrium position and the perturbed position due to an external dynamic excitation, $x_G(t)$ are both presented in Fig. 3.3. A detailed description of this mechanical configuration can be, also, found in Sapountzakis et al. (2016) and Sapountzakis et al, (2017). According to Fig. 3.3, the proposed system comprises of two symmetric linear pre-compressed horizontal springs, k_H. These springs support an additional mass, k_o through an articulated mechanism.

In order to calculate the value of negative stiffness produced by this pair of positive stiffness springs, the ensuing procedure is followed:

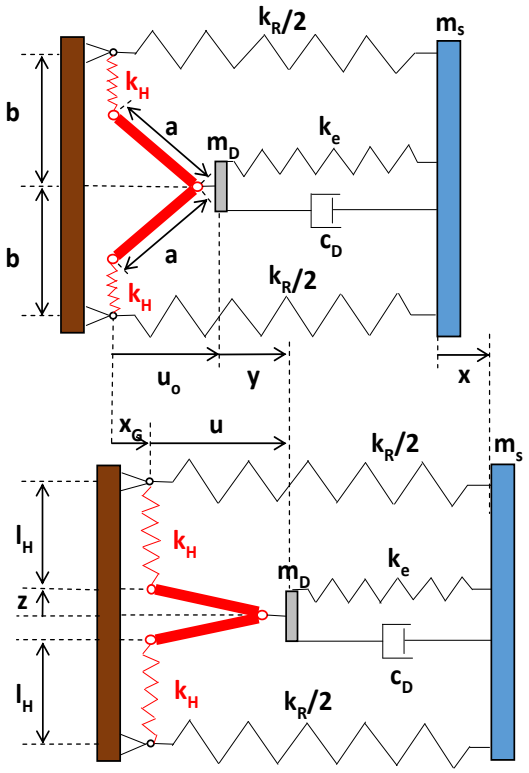

Figure 3.3: Schematic representation of the proposed configuration 1 (plan view).

First, the energy due to the deformation of the springs, k_H is calculated as

$$U_N(u) = 2\frac{1}{2}k_H\left(l_H - l_{HI}\right)^2 \tag{3.3.1}$$

where

$$l_H = b - \left(a^2 - u^2\right)^{1/2} \tag{3.3.2}$$

Then, the elastic non-linear force corresponding to the negative stiffness is given as

$$f_N(u) = \frac{\partial U_N}{\partial u} = \frac{\partial U_N}{\partial u_D} = -2k_H\left(1 + \frac{l_{HI} - b}{\sqrt{a^2 - u^2}}\right)u = -2k_H\left[1 + c_I\frac{1}{\left(1 - u^2/a^2\right)^{1/2}}\right]u \tag{3.3.3}$$

where

$$u = u_o + u_D \tag{3.3.4a}$$

$$c_I = (l_{HI} - b)/a \tag{3.3.4b}$$

Finally, the value of negative stiffness produced by each pair of linear pre-compressed horizontal springs, k_H is given by

$$k_N = \frac{\vartheta f_N}{\vartheta u} = \frac{\vartheta f_N}{\vartheta u_D} = -2k_H \left[1 + c_I \frac{1}{\left(1 - u^2/a^2\right)^{3/2}} \right] \tag{3.3.5}$$

In Eqs. (3.3.2), (3.3.3), (3.3.4b) and (3.3.5), a and b are geometrical parameters, as defined in Fig. 3.3., while l_{HI} denotes the initial length of the undeformed springs, k_H.

The calculation of the values of k_H, l_{HI}, a, b and u_o, that control the amount of negative stiffness provided by the proposed configuration depends on the mechanical characteristics of the system and the springs – a detailed description of which is out of the scope of the current project - as well as on physical limitations imposed by the structure to which the system is going to be implemented. For instance, in order for the manufacturing of the pre-compressed springs, k_H to be feasible and within a realistic range, the maximum absolute displacement, u_D of the internal mass, m_D of the mechanism should not exceed 70 cm. At this point, it should be noticed that, since the upper value of negative stiffness provided by this system is bounded due to these manufacturing limitations, similar mechanisms of this kind can be placed in parallel in the structure in view of obtaining the desired negative stiffness effect.

Further information on the implementation of such a mechanism to a structure, as part of the KDamper concept (Chapter 4) is given in Chapter 6, where specific test cases and numerical applications on bridge structures are presented.

3.3.2 Proposed Configuration 2 – Inverted Pendulum

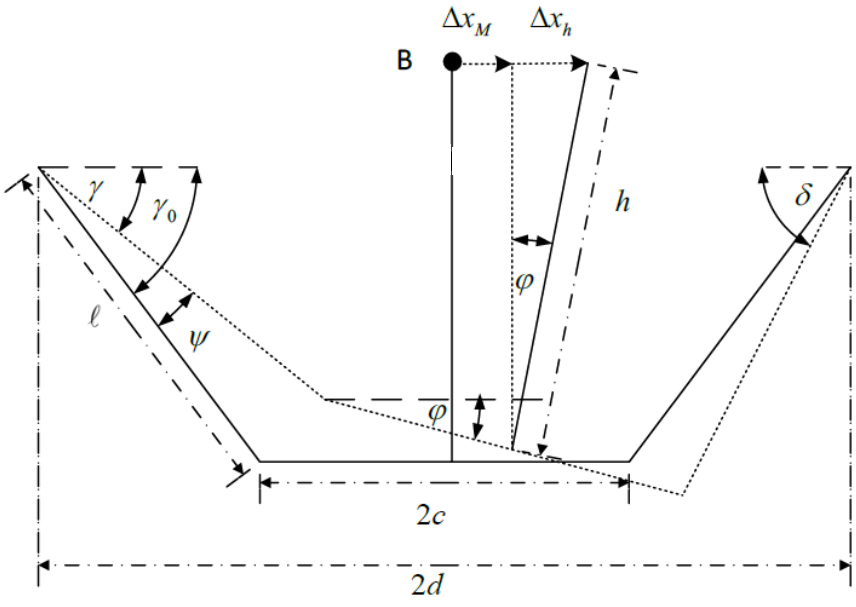

Figure 3.4: Schematic representation of the proposed configuration 2 (inverted pendulum).

Considering an alternative solution to the proposed configuration 1, the mechanism depicted in Fig. 3.4 is, also, recommended. Taking into account the characteristics and features of rocking objects (Housner, 1963), the configuration of Fig. 3.4 comprises of an additional I-shaped mass, m_D (Fig. 3.5)

that acts as an inverted pendulum. In an effort to explain better these two figures, it should be clarified here that the outline of the I-shaped mass, m_D of Fig. 3.5 is omitted from Fig. 3.4 for comprehensibility reasons. However, the line of length $2c$ of Fig. 3.4 coincides with the lower side of the outline of the I-shaped mass, m_D of Fig. 3.5, while point B of Fig. 3.4 represents the center of mass of the I-shaped mass, m_D, denoted as cm in Fig. 3.5.

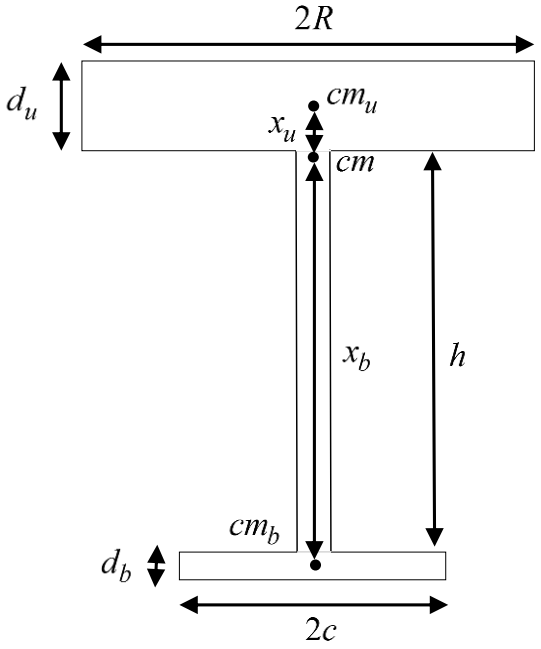

Figure 3.5: The I-shaped mass, m_D of the inverted pendulum.

The basic principles that control the mechanism's performance are discussed in the following. A detailed description of the kinematic and the dynamic analysis of the proposed system as well as of its design procedure can be, also, found in (Panagopoulos, 2017).

The inverted pendulum's performance is controlled by four basic dimensions, namely, c, d, l and h, depicted in Fig. 3.4. In order for the proposed configuration to produce a desired value of k_N, its geometric parameters should be consistent with the following procedure:

First, a relative negative stiffness coefficient can be estimated from Eq. (3.3.6)

$$k_{REL} = \frac{|k_N|}{-m_D g} \tag{3.3.6}$$

where, m_D is the additional mass and g is the gravitational acceleration which is considered equal to 10 m/s^2. After computing the value of k_{REL}, the four basic dimensions, c, d, l and h are calculated according to the procedure described in Panagopoulos (2017).

Subsequently, the total volume of the I-shaped mass, m_D is calculated from Eq. (3.3.7)

$$V_{tot} = m_D / \rho_{mat} \tag{3.3.7}$$

where ρ_{mat} stands for the density of the material used to realize the additional mass m_D. Then, taking into account the limitation imposed by Eq. (3.3.8), an initial value of d_b is assumed.

$$h + d_b + d_u < 4 \tag{3.3.8}$$

Once the value of d_b is assumed, the rest of the dimensions are computed according to Eqs. (3.3.9)

$$x_b = h + \frac{d_b}{2}, \qquad x_u = \frac{x_b}{Vtot / d_b \pi c^2 - 1}, \qquad d_u = 2x_u \ , \qquad R = \sqrt{\frac{x_b d_b}{x_u d_u}} c \tag{3.3.9a,b,c,d}$$

where c is the value of one of the four basic parameters, as mentioned in the previous. In the end, considering all calculated dimensions, the validity of limitation of Eq. (3.3.8) is checked.

Further information on the implementation of such a mechanism to a structure, as part of the KDamper concept (Chapter 4) is given in Chapter 6, where specific test cases and numerical applications on bridge structures are presented.

Chapter 4:
The KDamper Concept

In this chapter, a novel passive vibration absorption and damping concept, the KDamper concept is introduced. A description of the proposed device, incorporating negative stiffness elements, is given hereby, along with a detailed presentation of its main properties and features. The equations that control the performance of the KDamper are also included in the following.

4.1 INTRODUCTION

Exploiting the positive features of TMDs (Section 2.3) and of devices with negative stiffness elements (Chapter 3), a novel passive vibration absorption and damping concept, the KDamper concept, is introduced, in view of mitigating the effects of seismic excitations on structures. A KDamper device contains both positive and negative stiffness elements, arranged in appropriate geometrical configurations. An additional mass, operating as an energy dissipating mechanism, similarly to TMDs, and an artificial damper are also required. However, it differs from both the original SDoF oscillator, as well as from the known negative stiffness oscillators, due to the appropriate redistribution of the individual stiffness elements and the reallocation of the damping. The KDamper is also designed to present the same overall (static) stiffness as a traditional reference original oscillator, avoiding the main drawback of QZS oscillators, namely the drastic reduction of the structure's static stiffness and consequently, its bearing capacity. Furthermore, the KDamper overcomes the sensitivity problems of TMDs as the tuning is mainly controlled by the negative stiffness element's parameters.

As it has already been mentioned in Chapter 3 generally, the negative stiffness behaviour can be achieved by special mechanical designs involving conventional positive stiffness pre-stressed elastic mechanical elements, such as post-buckled beams, plates, shells and pre-compressed springs, arranged in appropriate geometrical configurations. In this project, the negative stiffness element is realized by a non-linear bistable element, which operates around an unstable equilibrium point. This bistable element takes the form of two symmetric linear horizontal springs, connected with the rest of the elements through an appropriate articulated mechanism (Fig. 3.3). Even though negative stiffness elements usually demonstrate an unstable behavior, the proposed device is designed to be statically and dynamically stable.

The design procedure described in the following was initially inspired by the optimum design of TMD devices as given by Den Hartog (1956). A similar approach was then initialized for the design of KDamper devices, as presented in Antoniadis et al. (2015) and Antoniadis et al. (2016). Once such a system is designed according to these two aforementioned approaches, it is shown to exhibit an extraordinary damping behavior. In this project, the proposed system is designed after the combining the main properties of Antoniadis et al. (2016) with the results of an optimization process – the specific features of which are going to be discussed in Chapter 5 – with limitations and criteria that are imposed by the selected mechanical configuration, responsible for the negative stiffness behavior, and the desired performance requirements of the isolated system. Similar approaches can be found in Sapountzakis et al. (2016) and Syrimi et al. (2017).

In the previously mentioned approaches, the KDamper has been successfully applied on bridge structures. A similar application on a typical single-pier concrete bridge will be also presented in Chapter 6. Initial approaches on the implementation of the KDamper concept, compared with the use of TMDs, to wind turbine towers can be found in Kapasakalis et al. (2017)

4.2 METHODOLOGY

4.2.1 Overview of the KDamper concept

Fig. 4.1 presents the basic layout of the vibration isolation and damping concept to be considered. The device is designed to minimize the response $x(t)$ of a SDoF system of mass m_s and static

stiffness k_o to a base excitation of $x_G(t)$. The SDoF system may be undamped or have a low initial damping ratio.

The first basic requirement of the KDamper is that the overall static stiffness of the system is maintained, as it is stated in Eq. (4.2.1), where k_R and k_e represent the stiffness coefficients of the conventional springs, k_N is the algebraic value of the stiffness coefficient of the negative stiffness element and k_o stands for the stiffness of an equivalent undamped SDoF system.

$$k_R + \frac{k_e k_N}{k_e + k_N} = k_o \tag{4.2.1}$$

In this way, the KDamper can overcome the fundamental disadvantage of the QZS oscillator, which is the reduction of the overall stiffness of the system that simultaneously limits the static loading capacity of the structure. Furthermore, the extraction of comparative results between the two systems (initial - SDoF and isolated one) is enabled.

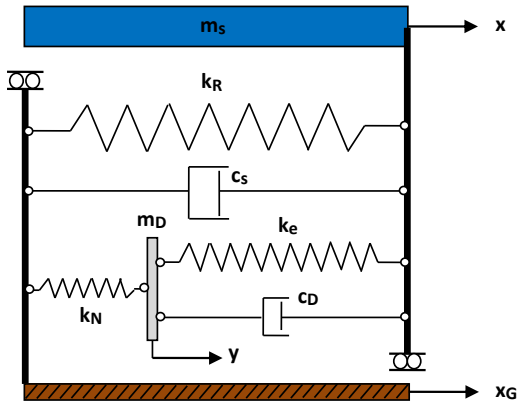

Figure 4.1: Schematic representation of the considered vibration absorption concept.

The equations of motion after the implementation of the KDamper are presented below

$$m_s\ddot{u}_s + (c_s + c_D)\dot{u}_s - c_D\dot{u}_D + (k_R + k_e)u_s - k_e u_D = -m_s\ddot{x}_G \tag{4.2.2a}$$

$$m_D\ddot{u}_D - c_D\dot{u}_s + c_D\dot{u}_D - k_e u_s + (k_e + k_N)u_D = -m_D\ddot{x}_G \tag{4.2.2b}$$

where

$$u_s = x - x_G \tag{4.2.3a}$$

$$u_D = y - x_G \tag{4.2.3b}$$

c_s is the initial's systems damping coefficient and c_D is the damping coefficient of the additional damper.

At this point, it should be mentioned that the KDamper essentially consists an indirect approach to increase the inertia effect of the additional mass m_D without, however, increasing directly the mass m_D itself.

4.2.2 Proposed design approach for the KDamper

As it is already mentioned in Section 4.1 of the current chapter, in this project the proposed design procedure combines features included in the approaches of Antoniadis et al. (2016), Sapountzakis et al. (2016) and Syrimi et al. (2017).

The device's behavior and consequently, the isolated system's dynamic performance, are controlled by three basic design parameters, μ, κ and ζ_D which are defined as follows:

$$\mu = m_D / m_s \tag{4.2.4a}$$

$$\kappa = -\frac{k_N}{k_e + k_N} \tag{4.2.4b}$$

$$\zeta_D = \frac{c_D}{2\sqrt{k_D m_D}} \tag{4.2.4c}$$

where m_s is the superstructure's mass, m_D is the additional mass of the KDamper, ζ_D is the damping ratio corresponding to the artificial damper, as shown in Fig. 4.1, and k_D is given by Eq. 4.2.5 for the KDamper.

$$k_D = k_e + k_N \tag{4.2.5}$$

The three parameters μ, κ and ζ_D, as defined in Eqs. (4.2.4), are design variables whose values are obtained from the results of an optimization process. Further explanation on this process, regarding the employed optimization algorithm, the design variables and their limits, and consequently, on the values of μ, κ and ζ_D is given in Chapter 5 of the current project. The effect of each one of the aforementioned parameters on the device's and by extent, on the isolated systems behavior is described in the following section of the current chapter, referring to the basic properties of the KDamper.

According to Antoniadis et al. (2016), there is a fourth parameter, required to acquire a complete and accurate design of the KDamper device. That is the frequency ratio ρ which is defined as

$$\rho = \omega_D / \omega_o \tag{4.2.6}$$

where

$$\omega_o = \sqrt{k_o / m_s} \tag{4.2.7a}$$

$$\omega_D = \sqrt{k_D / m_D} \tag{4.2.7b}$$

However, ρ is not an independent parameter, but its value depends on the values of μ and κ and consequently, ρ is not considered a design variable. More specifically, for each set of the parameters μ and κ, the value of ρ is derived from

$$\rho(\kappa, \mu) = \sqrt{-C_\rho / B_\rho} \tag{4.2.8}$$

where C_ρ and B_ρ are algebraic coefficients calculated following the procedure described in Appendix A. The final value of ρ according to Appendix A is given by

$$\rho(\kappa,\mu)=\sqrt{\frac{1}{(1+\mu+\kappa\mu)(1+\mu)-\kappa^2\mu}} \tag{4.2.9}$$

Once the values of the four basic parameters μ, κ, ζ_D and ρ are determined, the values of the KDamper's elements can be finally, after some algebraic manipulations, presented thoroughly in Appendix B, obtained from the following relations

$$\frac{k_N}{k_o}=\kappa_N=-\kappa\mu\rho^2 \tag{4.2.10a}$$

$$\frac{k_e}{k_o}=\kappa_e=(1+\kappa)\mu\rho^2 \tag{4.2.10b}$$

$$\frac{k_R}{k_o}=\kappa_R=1+\kappa(1+\kappa)\mu\rho^2 \tag{4.2.10c}$$

$$m_D=\mu m_s \tag{4.2.10d}$$

$$c_D=2\zeta_D\sqrt{(k_e+k_N)m_D} \tag{4.2.10e}$$

Eq. (4.2.10e) is derived after substituting Eq. (4.2.5) into Eq. (4.2.4c).

4.2.3 Basic properties of the KDamper device

As it has already been noted in the previous, the device's behavior is controlled by the three design parameters, μ, κ and ζ_D. As far as parameters μ and ζ_D are concerned, the bigger their value is, the better the dynamic performance of the isolated system. This behavior can be explained by the fact that a bigger additional mass leads to an increase of inertia forces whereas a bigger value of damping ratio, ζ_D (defined in Eq. (4.2.4c)) of the artificial damper, as shown in Fig. 4.1, facilitates the reduction of displacements. Although bigger values of these two parameters seem to be necessary to obtain an improved dynamic performance, there are, usually, upper limits that need to be considered. These upper limits are imposed by the nature of each structure, the constructability and applicability of the device and of course, the final structure's cost. For example, when dealing with structures where the value of m_s is extremely big, such as bridges, parameter μ is cannot exceed a value of 15-20%, in order for the additional mass to have a realistic value that can be manufactured with low cost materials and placed easily on the structure. Thus, a careful choice satisfying both the desired effects on structure's response and the ability to construct and place the device should be made. It is reminded that in this effort, the value of parameter μ is selected arbitrarily by the user whereas the value of the damping ratio ζ_D is obtained from the results of the optimization process, presented in Chapter 5.

Considering the parameter κ, it should be mentioned here that increasing its value has a number of implications in the design of the KDamper. First, high stiffness values result, as presented in Figs. 4.2-4.4. In addition, as observed in Fig. 4.5, when κ reaches $\kappa_{\max}$ the frequency ratio ρ tends to infinity. The value of κ is, also, responsible for the shift of the eigenfrequency (and by extension the shift of the eigenperiod) of the isolated system. This fact can be observed in Figs. 4.6 and 4.7, where the effect of the value of κ to the transfer function of the isolated system is depicted, in terms of acceleration and in terms of displacement, respectively.

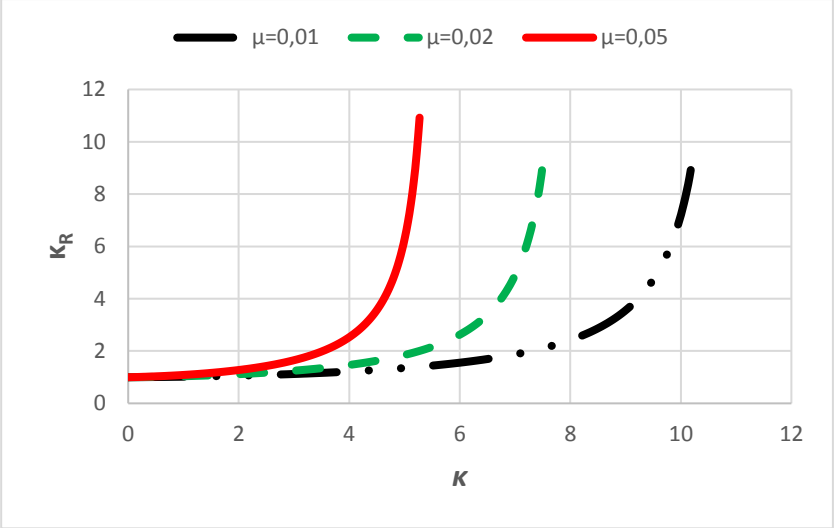

Figure 4.2: Increase of the value of stiffness coefficient k_R by increasing κ (in terms of ratio κ_R).

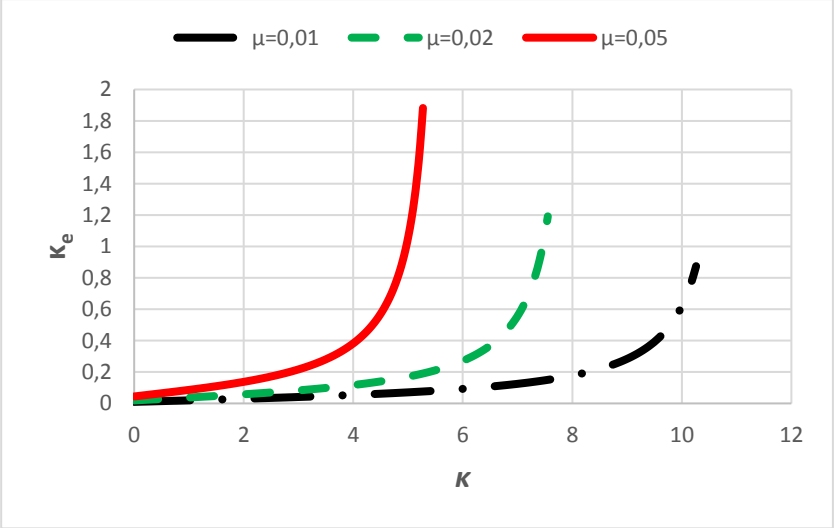

Figure 4.3: Increase of the value of stiffness coefficient k_e by increasing κ (in terms of ratio κ_e).

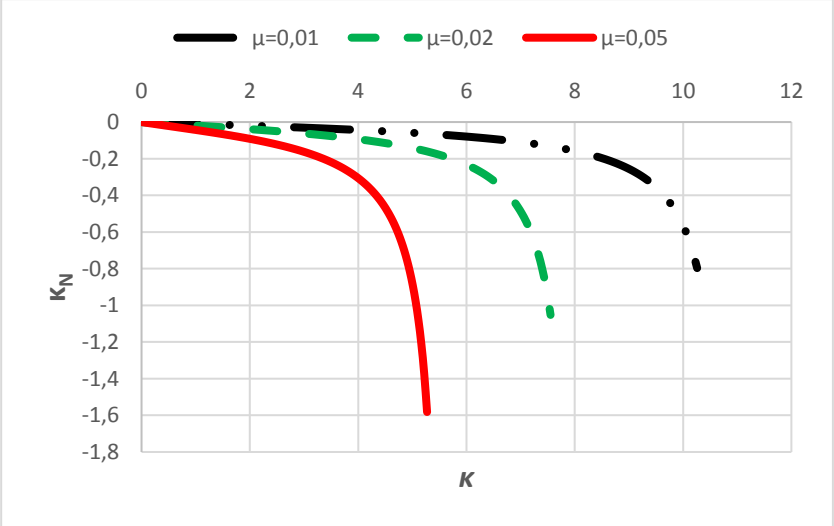

Figure 4.4: Increase of the value of negative stiffness coefficient k_N by increasing κ (in terms of ratio κ_N).

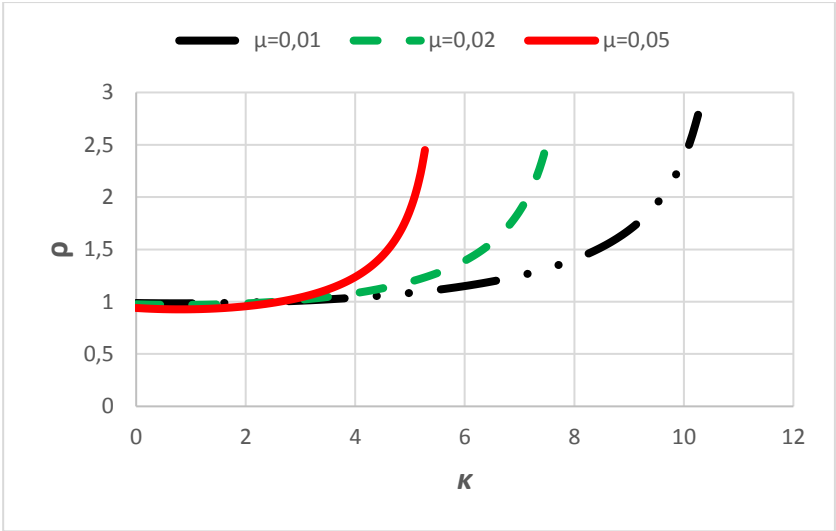

Figure 4.5: Variation of the KDamper's parameters μ and κ over the frequency ratio $\rho = \omega_D / \omega_o$.

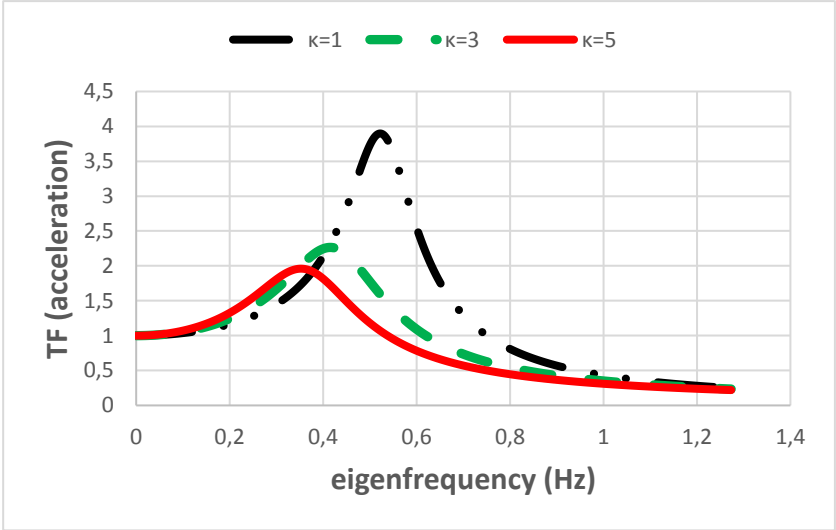

Figure 4.6: Transfer function of the isolated system in terms of acceleration.

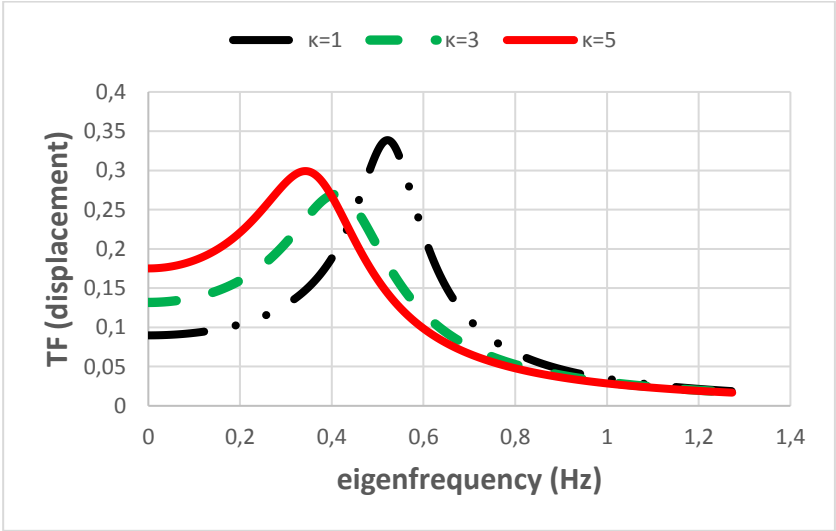

Figure 4.7: Transfer function of the isolated system in terms of displacement.

Taking a closer look to Figs. 4.6 and 4.7, the following remark can be extracted: values of the isolated system's eigenfrequency that are close to 0.4 Hz, lead to systems that exhibit an improved dynamic behavior in terms of acceleration and in terms of displacement as well. On the contrary, eigenfrequency values lower than 0.4 Hz result in systems where the reduction of acceleration is accompanied by an undesirable increase of displacements. This remark is used in this effort as a second check, in order to prove that the optimization algorithm has achieved the best possible solution and the device has been successfully designed for seismic isolation (Chapter 6).

Increasing the stiffness and especially k_N, may endanger the static stability of the structure. Although k_N is selected according to Eq. (4.2.1) to ensure the system's static stability, variations of k_N result in practice due to various reasons, such as temperature variations, manufacturing tolerances, or non-linear behavior, since almost all negative stiffness designs result from unstable non-linear systems. Consequently, an increase of the absolute value of k_N by a factor ε may lead to a new value of k_{NL} where the structure becomes unstable, given by

$$k_R + \frac{k_e k_{NL}}{k_e + k_{NL}} = 0 \Leftrightarrow k_{NL} = -\frac{k_R k_e}{k_R + k_e} = (1+\varepsilon) k_N \tag{4.2.11}$$

Substitution of Eqs. (4.2.10a), (4.2.10b) and (4.2.10c) into Eq. (4.2.11) leads to the following estimate for the static stability margin ε

$$\varepsilon = \frac{1}{\kappa\left[1+(1+\kappa)^2 \mu\rho^2\right]} \tag{4.2.12}$$

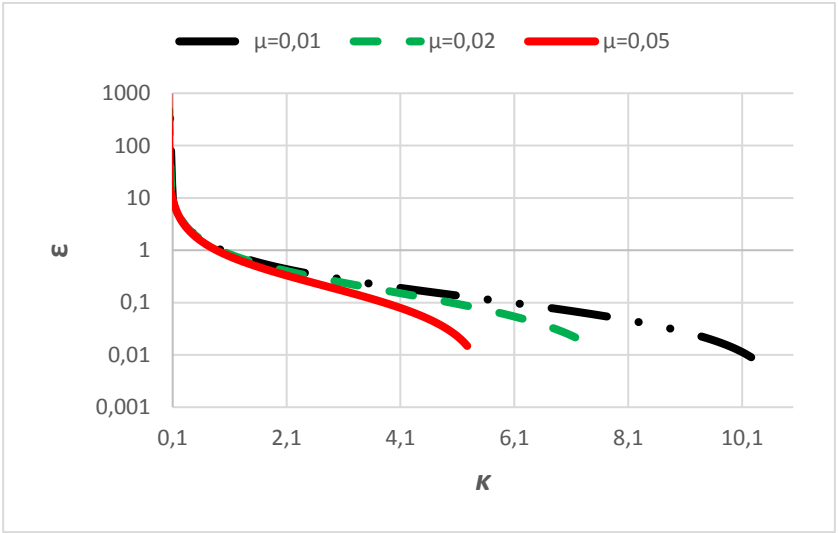

Figure 4.8: Variation of the KDamper's parameters μ and κ over the static stability margin ε.

Fig. 4.8 presents the variation of ε over κ and μ. As it can be observed from Eq. (4.2.12) and Fig. 4.8, the increase of the negative stiffness of the system is upper bounded by the static stability limit of the structure, where ε tends to zero. The increase of the value of κ is, consequently, upper limited by a value of $\kappa_{\max}$. In practice, the value of $\kappa_{\max}$ can be calculated by a Goal Seek command

with the condition that ε is equal to zero. It is reminded here, that the final value of parameter is obtained from the results of the optimization process, described in Chapter 5.

Chapter 5: Optimization Process

In this chapter, the optimization process, on whose results the design of the KDamper is based, is described. More precisely, the optimization algorithm, the design variables, their limits and the selected objective function are presented thoroughly in the following.

5.1 INTRODUCTION

5.1.1 The need for optimization

Regarding the basic principles of seismic isolation, as discussed in Section 1.2 of this effort, as well as the properties of the KDamper concept and the physical and manufacturing limitations that might occur during its implementation (e.g. upper limit of internal DoF displacement), the need to optimally design the KDamper device becomes more and more obvious.

5.1.2 Genetic and Metaheuristic Algorithms

Heuristic optimization techniques based on simulation methods have made their appearance as a mean to overcome accuracy deficiencies of conventional mathematical tools (linear, non-linear or dynamic programming) when employed for the solution of complex optimization problems. By 1970, numerous heuristic algorithms have been developed, imitating natural phenomena. Among others, simulated annealing (SA), (Kirkpatrick et al., 1983), tabu search (TS), (Glover, 1977) and evolutionary algorithms (EA) enlist.

Following the path of the above-mentioned techniques, genetic algorithms (GA) are search algorithms based on natural selection and population genetics. The theory of GA was proposed by Holland (1975) and further developed by Goldberg (1989). The simple GA comprises of three operators, namely, reproduction, crossover and mutation. Reproduction is a process of survival-of-the-fittest selection, crossover represents the partial swap between two parents to produce an offspring and, finally, mutation is the occasional random inversion of bit values, generating non-recursive offspring. The main feature of GA that separates it from traditional optimization methods as well as from heuristic algorithms, is the capability to simultaneously evaluate many solutions within an iteration. This precious advantage enables a wide range of search areas, potentially avoiding convergence to non-global optima.

Towards the same direction, numerous advanced metaheuristic algorithms have been proposed. Metaheuristic algorithms are not problem specific, a feature that renders them suitable choices for various optimization problems. They are inspired by natural phenomena and processes. Moreover, they provide approximate, non-deterministic solutions that are good enough for practical purposes (e.g. preliminary dynamic design of structures) in short amounts of time.

In 2001, Geem et al., proposed a novel metaheuristic algorithm, harmony search algorithm (HS) inspired by musical harmony. Similarly, to the GA, HS exhibits numerous positive characteristics that render it suitable for various optimization problems including the traveling salesman problem (Geem et al., 2001), optimization of data classification systems (Wang et al., 2009), pipe network design (Geem et al., 2002) and generalized orienteering problem (Geem et al., 2005). Considering the solution of structural problems, HS has been successfully applied to the optimum design of truss structures (Lee and Geem, 2004), steel sway frames (Saka, 2009) and grillage systems (Erdal and Saka, 2009). Recently, HS has been employed for the optimum design of the implementation of TMDs to multistory buildings (Nigdeli et al., 2014), (Nigdeli and Bekdas, 2017). An initial approach to optimize the design of a KDamper device, similar to the one adopted hereby, can be found in Syrimi et al., (2017). A detailed description of HS algorithm, along with its special features and unique properties is given in the following sections of the current chapter. Moreover, the HS optimization process for the design of the KDamper device (Chapter 4) is thoroughly explained to ensure better understanding of the numerical applications presented in Chapter 6 of this project.

5.2 HARMONY SEARCH ALGORITHM AND OPTIMIZATION PROCESS

5.2.1 Harmony Search (HS) Algorithm

As it has already been mentioned in Section 5.1 of the current chapter, HS algorithm exhibits certain useful characteristics and properties that render it a suitable and powerful tool for the solution of complex mathematical and engineering problems. At the same time, HS appears to be a promising alternative to conventional optimization techniques, especially considering problems where the latter cannot be applied.

In the following, the positive properties of HS algorithm are described. First of all, HS can handle problems with both discrete and continuous variables (Lee et al., 2005), (Lee and Geem, 2005) and is characterized by the distinguishing features of algorithm simplicity and search efficiency. Since it is not a hill-climbing algorithm, the probability of becoming entrapped to a local optimum is significantly reduced. Moreover, it uses a stochastic random search instead of a gradient search, as other metaheuristic algorithms do, gaining in simplicity. Stochastic derivatives are useful for a number of scientific and engineering problems where mathematical derivatives cannot be calculated or easily treated (Geem, 2008) and also serve to the reduction of the required number of iterations.

A summary of the aforementioned HS distinguishing features and advantages is presented in the flowchart of Fig. 5.1.

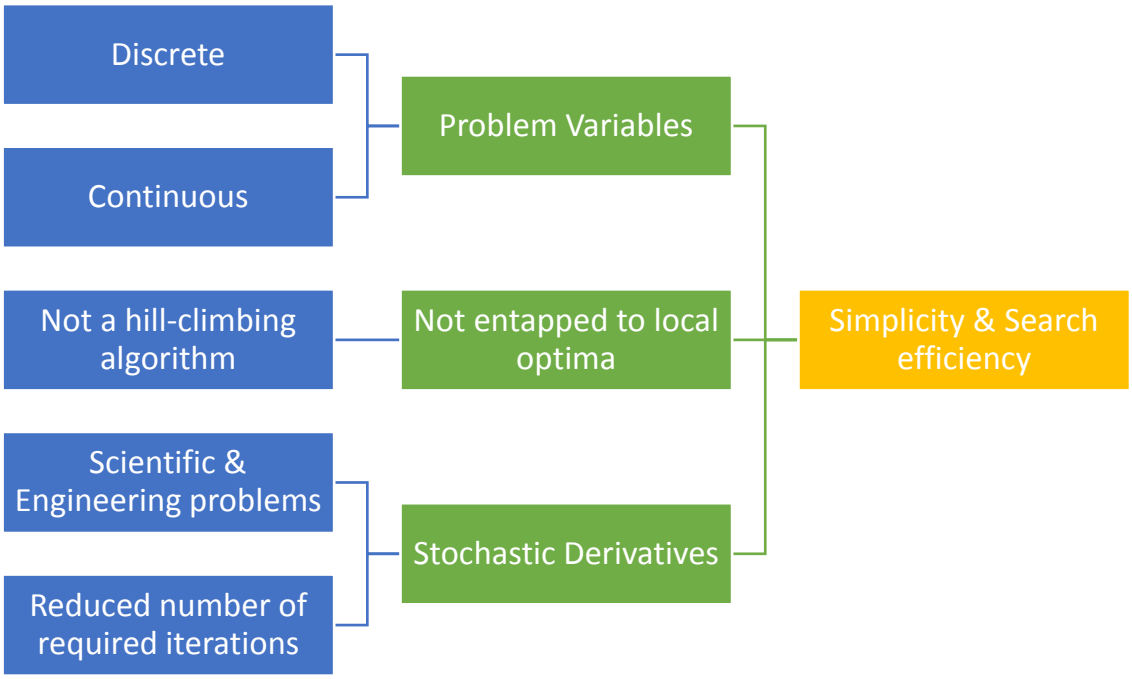

Figure 5.1: Distinguishing features and advantages of the HS algorithm.

A detailed description of the HS algorithm can be found in Geem et al., (2001), Nigdeli et al., (2014), Nigdeli and Bekdas, (2017) and Gao et al., (2015). However, the four basic steps of the algorithm are, also, cited in the following:

Step 1: Initialization of the HS Memory matrix (HM). HM matrix contains vectors which represent possible solutions to the examined optimization problem. The initial HM matrix is created using randomly generated solutions. For an n-dimension problem, HM has the form

$$HM = \begin{bmatrix} x_1^1, x_2^1, \ldots, x_n^1 \\ x_1^2, x_2^2, \ldots, x_n^2 \\ \cdot \\ \cdot \\ \cdot \\ x_1^{HMS}, x_2^{HMS}, \ldots, x_n^{HMS} \end{bmatrix} \tag{5.2.1}$$

where $\left[x_1^1, x_2^1, \ldots, x_n^1\right]$ $\left(i = 1, 2, \ldots, HMS\right)$ is a solution candidate. HMS is typically set to values between 50 and 100. For every solution vector of the HM matrix, the value of the objective function is calculated.

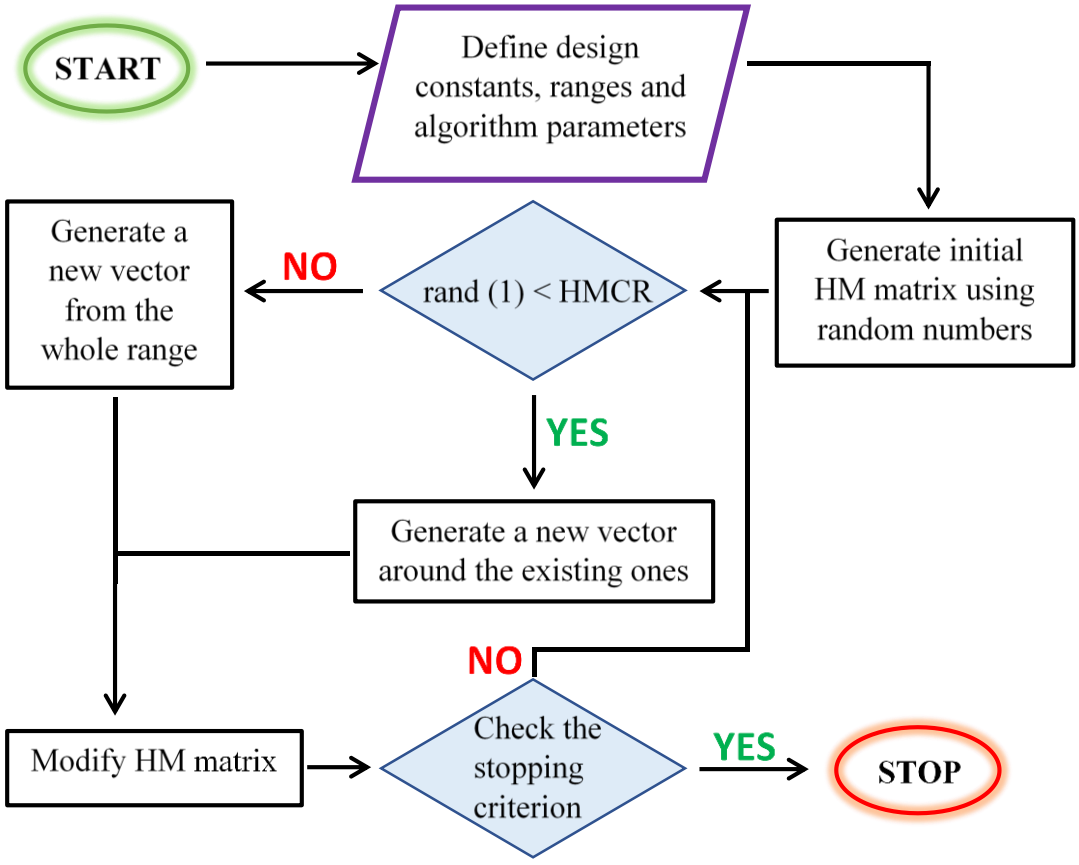

Figure 5.2: Flowchart of the HS algorithm.

Step 2: Improvisation of a new solution, $\left[x_1', x_2', \ldots, x_n'\right]$, from the HM. Each one of the components of this new solution, x_j', is obtained based on the Harmony Memory Considering Rate (HMCR), defined as the probability of selecting a component among the HM members. Therefore, the value of 1 – HMCR is the probability of generating a new component randomly. When x_j' is chosen

from the HM matrix, it is further mutated according to the Pitching Adjusting Rate (PAR), that determines the probability of a candidate from the HM to be mutated.

Step 3: Update of the HM matrix. The value of the objective function of the new solution, obtained in Step 2, is calculated and compared to the ones that correspond to the original HM matrix vectors. If it results in a better fitness than that of the worst member in the HM, it will replace that one. In the typical case of a minimization optimization process, the new solution replaces a member of the HM matrix, only if that member has a bigger value of objective function than the new one. If there are more than one members in the HM with larger values of the objective function that the new solution, the one with the higher value is replaced. Otherwise, the new solution is eliminated and HM matrix remains intact.

Step 4: Repetition of Steps 2 and 3 until a preset termination criterion is met. A commonly used termination criterion is the maximum number of total iterations.

The flowchart of the proposed HS algorithm is presented in Fig. 5.1.

5.2.2 Proposed Optimization Process

The features of the examined optimization problems can be derived according to the procedure thoroughly presented in Syrimi et al. (2017). Some brief and useful comments are, also, noted hereby. The main difference lies on the objective function and the imposed constraints which are described in the following.

Starting from the design variables, the three parameters that control the device's performance μ, κ, and ζ_D are selected. The allowable range of values for these parameters is defined by determining their limits, given in Table 5.1. At this point, it is reminded that the choice of the parameter limits lies on safety, stability and manufacturing aspects that need to be taken into account. Concerning the parameters inherently involved in the HS algorithm, values commonly found in relative literature are adopted (Table 5.2). Similarly, in this effort, the maximum number of total iterations is selected as the termination criterion.

Table 5.1: Variable design limits.

	$\boldsymbol{\mu}$	$\boldsymbol{\kappa}$	$\boldsymbol{\zeta_D}$
min	0.01	2.234	0.01
max	0.10	2.831	0.50

Table 5.2: Values of the HS algorithm parameters.

HMS	**HMCR**	**PAR**
75	0.5	0.1

In view of finding the optimum solution, the Root Mean Square (RMS) of the deck's absolute kinetic energy for three seismic excitations is selected as the objective function. Precisely, three different earthquake excitations that took place in three different locations of Greece, namely, in Athens, in Aigio and in Kalamata are employed. However, in order for the design to be as close as possible to Eurocode seismic requirements, the original earthquake records – from now on referred to

as origin records – were scaled so that each record's response spectrum approximately matches the EC8 design spectrum (Spectrum type 1, Soil type B, Zone 3). The earthquake records were scaled using SeismoMatch software (Seismosoft, 2016). The resulting earthquake records will be referred to as matched records. In Figs 5.3a, 5.4a and 5.5a, the frequency content of both origin and matched records are presented for Athens, Aigio and Kalamata earthquakes, respectively. The response spectrum of the origin records as well as the corresponding one of the matched records, compared to the EC8 spectrum, are depicted in Fig. 5.3b for Athens earthquake, in Fig. 5.4b for Aigio earthquake and in Fig. 5.5b for Kalamata earthquake.

Finally, the following constraint is imposed: the value of deck's relative displacement is set lower than 0.15 m.

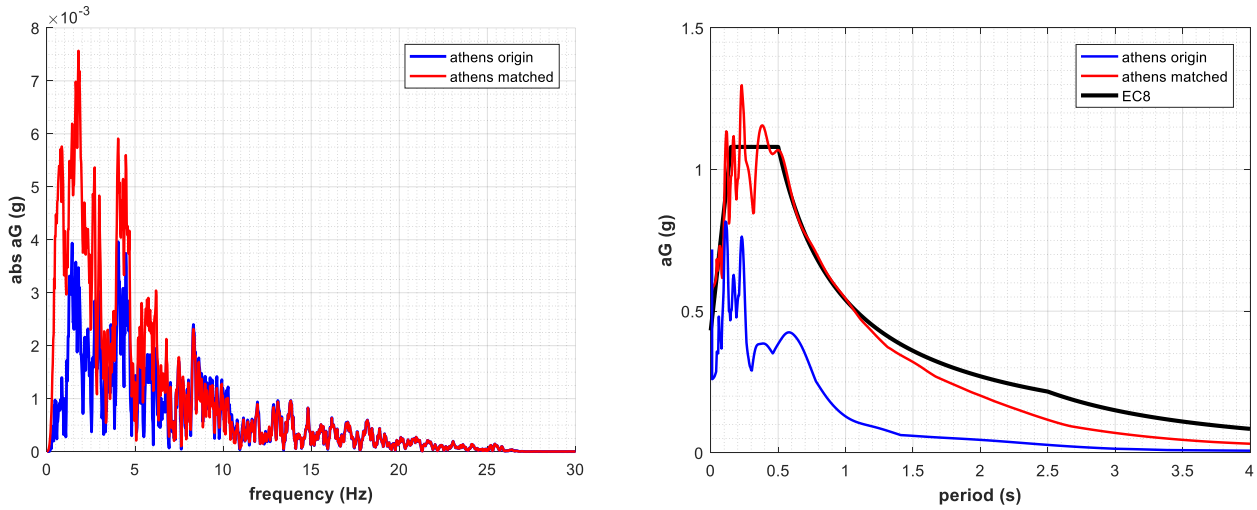

(a) (b)

Figure 5.3: (a) Frequency content of Athens origin and matched earthquake records. (b) Response spectra of Athens origin and matched earthquake records compared to the EC8 response spectrum.

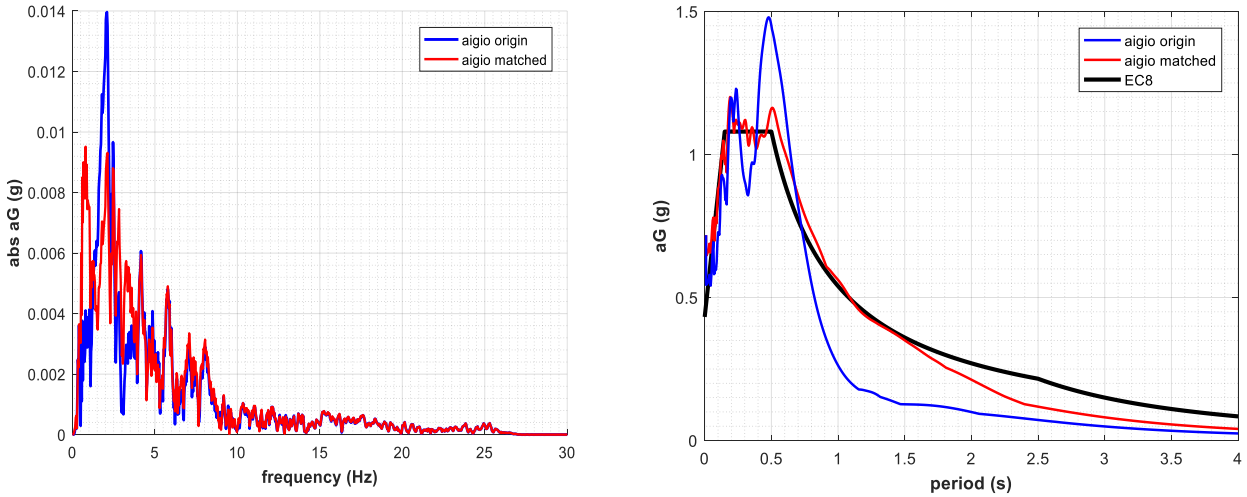

(a) (b)

Figure 5.4: (a) Frequency content of Aigio origin and matched earthquake records. (b) Response spectra of Aigio origin and matched earthquake records compared to the EC8 response spectrum.

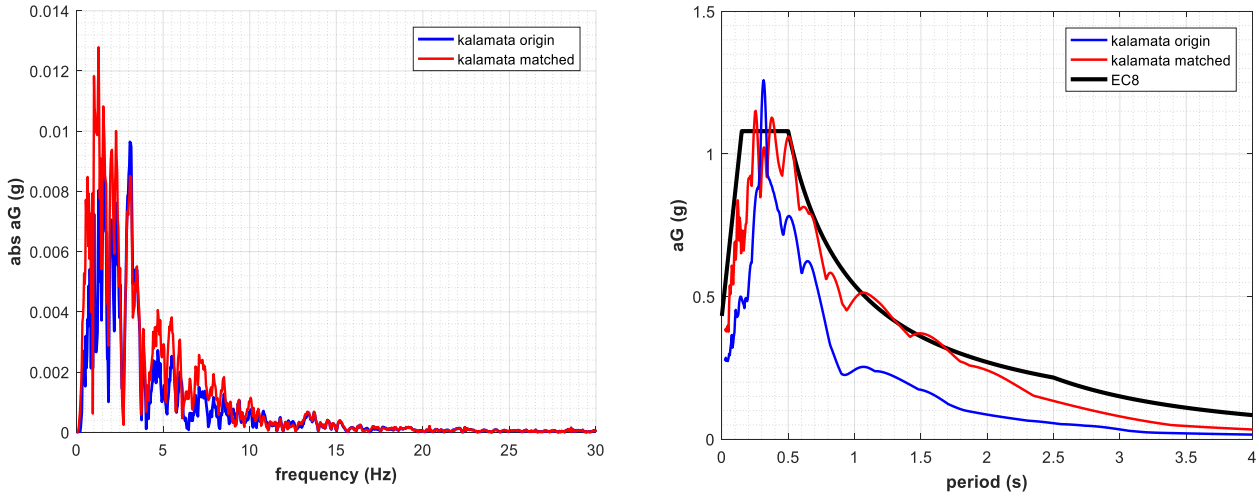

(a) (b)

Figure 5.5: (a) Frequency content of Kalamata origin and matched earthquake records. (b) Response spectra of Kalamata origin and matched earthquake records compared to the EC8 response spectrum.

Chapter 6: Numerical Applications

In this chapter, three different numerical applications, towards the implementation of the KDamper concept to bridge structures, are presented. The corresponding dynamic analysis results, validate not only the accuracy and effectiveness of the proposed seismic effects' mitigation method but, also, the robustness of the aforementioned optimization procedure.

6.1 INTRODUCTION

In an effort to implement the proposed negative stiffness based concept, the KDamper concept, to bridge structures and examine their behavior and dynamic performance, the three following numerical applications have been considered. Precisely, two typical concrete bridges, the first with two spans and solid piers and the second with three spans and hollow piers, have been tested under different types of dynamic loads as well as earthquake excitations. For each bridge one of the proposed configurations of Chapter 3 has been chosen, taking into account the applicability and other manufacturing aspects at each case. When possible, the design was carried out through the optimization process described in Chapter 5, using the Harmony Search (HS) algorithm. The corresponding results, presented in the following sections of the current chapter, validate not only the accuracy and effectiveness of the proposed seismic effects' mitigation method but, also, the robustness of the aforementioned optimization procedure.

6.2 NUMERICAL APPLICATION 1

6.2.1 Test case considered

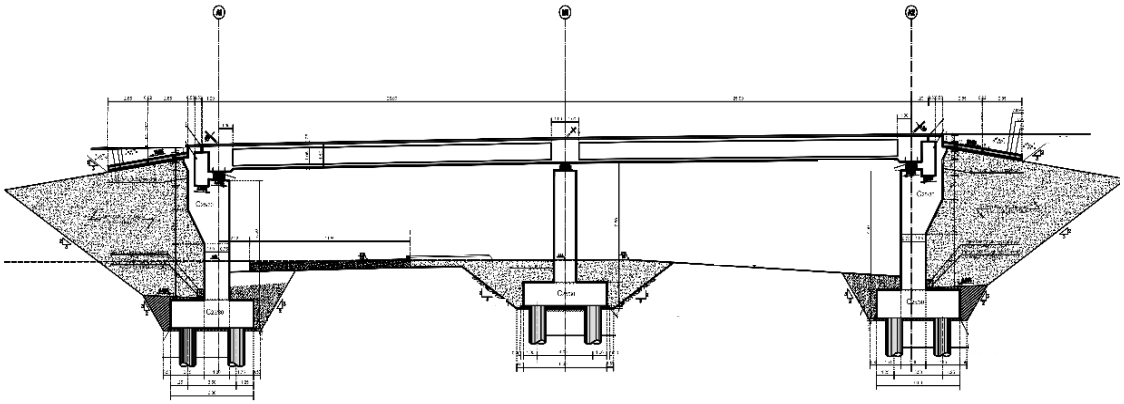

(a)

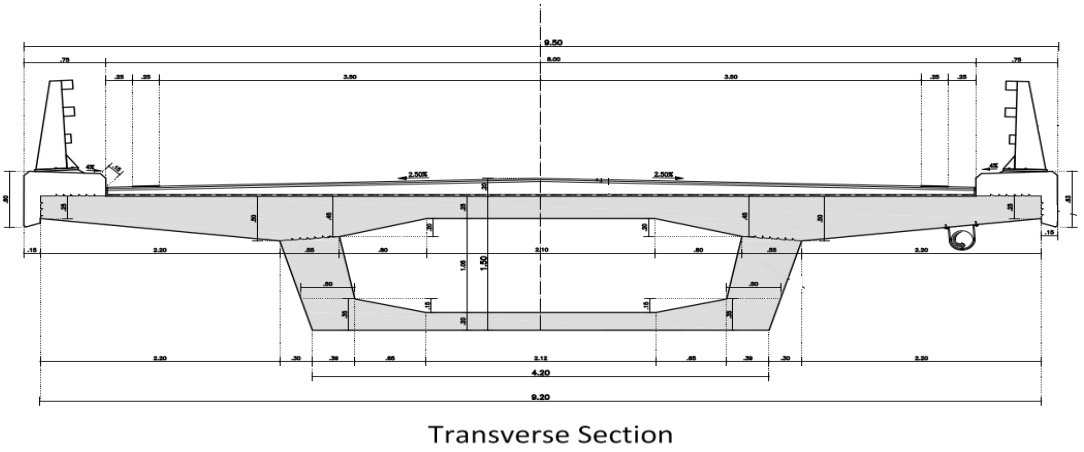

(b)

Figure 6.1: Schematic representation of the bridge considered. (a) Longitudinal section, (b) Transverse section.

For the first numerical application, the typical two-span concrete bridge of Fig. 6.1 has been considered. The length of each span equals to 25m and the deck is 9.50m wide. Simple elastomeric bearings support the deck. The dynamic characteristics and eigenfeatures of the initial SDoF system are given in Table 6.1.

Table 6.1: Dynamic characteristics and eigenfeatures of the initial SDoF system.

Mass, m_s (tn)	**k_o (kN/m)**	**Period, T (s)**	**Frequency, f (Hz)**	**Damping factor, c_s, (kNs/m)**	**Damping ratio, ζ (%)**
723.9	13650	1.45	0.70	314.3443	5

where, k_o is the total stiffness of the elastomeric bearings, which are going to be replaced by the KDamper devices. The bridge's pier is considered to be stiff enough to be neglected.

In this particular test case, the proposed configuration 1, as described in Section 3.3.1 of the current effort, is employed. Six KDamper device are used to replace the conventional bearings, two above each one of the abutments and the pier. It is reminded that this is possible since each KDamper device operates in parallel with the others. The resulting, after the implementation of the KDamper concept, isolated 2DoF system undergoes the optimization process as presented in Section 5.2.2. After designing the KDamper device, the system is subjected to the three earthquake excitations, also used during the aforementioned optimization procedure. In addition, the KD system is subjected to a free vibration with initial conditions, aiming to calculate its damping ratio. For every time history analysis that takes place, the Newmark-β method is used. The obtained results regarding both the design and the dynamic analysis of the bridge considered are presented in the following.

6.2.2 Results

The optimum values of the design variables, obtained using the HS optimization process are presented in Table 6.2. Then, the values of the KDamper elements coefficients are computed according to the procedure described in Chapter 4 and Appendix B (Table 6 .3). The values of the proposed configuration 1 parameters, which was employed for this numerical application, are given in Table 6.4. The dynamic eigenfeatures of both the initial and the isolated systems are given in Table 6.5, whereas comparative results between the two aforementioned systems for each one of the three earthquake excitations can be found in Table 6.6, in terms of the deck's absolute acceleration and relative displacement.

Table 6.2: Optimum values of the design variables.

μ	κ	ζ_D
0.0657	2.2617	0.1165

Table 6.3: Resulting values of the KDamper elements' constants (for each one of the six KDamper devices).

m_D (tn)	**c_D (kNs/m)**	**k_R (kN/m)**	**k_e (kN/m)**	**k_N (kN/m)**
7.93	8.20	3426.67	509.2	-353.1

Table 6.4: Resulting values of the proposed configuration 1 parameters (for each one of the six KDamper devices).

k_H (kN/m)	l_{HI} (m)	a (m)	b (m)	u_o (m)
174.47	1.37	0.65	1.4	0.005

Table 6.5: Dynamic eigenfeatures of both the initial and the isolated system.

	Period, T (sec)	Frequency, f (Hz)	Damping ratio, ζ (%)
Initial system	1.45	0.70	5
Isolated system	2.28	0.4	24.6

Table 6.6: Deck's absolute accelerations and relative displacements of both systems.

	Initial system		Isolated system	
	a_{abs} (m/s^2)	u_{rel} (m)	a_{abs} (m/s^2)	u_{rel} (m)
Athens	3.33	0.177	3.11	0.137
Aigio	3.67	0.195	2.76	0.119
Kalamata	3.69	0.196	3.03	0.122

Taking a closer look to the results obtained from the previous analyses, it is observed, that the isolated system exhibits an overall improved behavior, in both terms of deck's absolute acceleration and deck's relative displacement. An almost 5 times higher damping ratio is achieved, as shown in Table 6.5. Finally, the frequency of the isolated system, whose control parameters have been extracted from the HS optimization procedure, results equal to 0.4 Hz. This fact justifies the effectiveness of the employed optimization algorithm, since the positive outcome of structures with eigenfrequency close to the aforementioned value has been, also, noticed in Section 4.2.3, when the KDamper device's properties were discussed.

6.3 NUMERICAL APPLICATION 2

6.3.1 Test case considered

For the second numerical application, a typical three span concrete bridge is considered. A longitudinal section of the bridge and a transverse section of the deck are given in Figs. 6.2 and 6.3, respectively, whereas the section of the hollow piers is given in Fig. 6.4. More specifically, the bridge consists of three spans of length – starting from the left to the right - 29.754 *m*, 36.034 *m* and 29.779 *m*, respectively (total length = 95.567 *m*). The two piers have a rectangular 4x5 hollow section (4 *m* in the longitudinal direction and 5 *m* in the transverse direction) and thickness equal to 0.60 *m*. As a result, the free area inside each hollow pier is a rectangular 2.8x3.8 one. The left pier is 27 *m* high, while the right has a height of 24 *m*. The bridge deck is supported by 16 ALGABLOC NB4 400x500x196(88) elastomeric bearings (4 on each pier or abutment) with a horizontal stiffness of 2045 *kN/m* each. In this initial effort to implement the KDamper concept with inverted pendulum, the piers are considered stiff enough to be neglected. The dynamic eigenfeatures of this system – from now on referred to as the initial system/structure – are presented in Table 6.7.

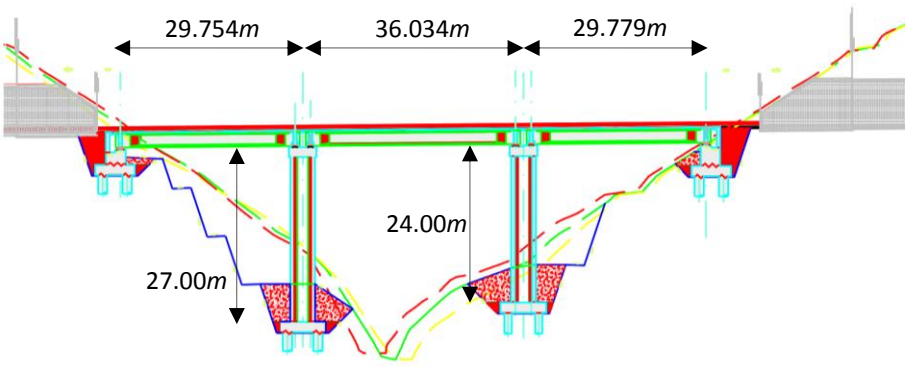

Figure 6.2: Longitudinal section of the bridge considered.

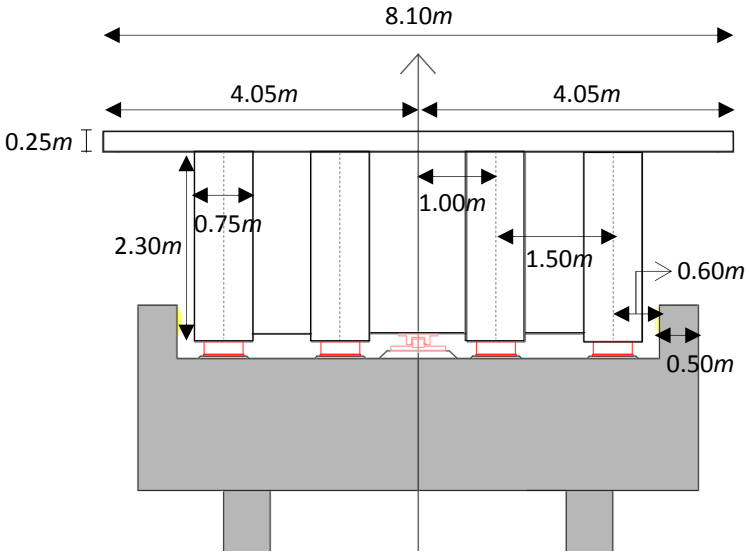

Figure 6.3: Transverse section of the bridge's deck.

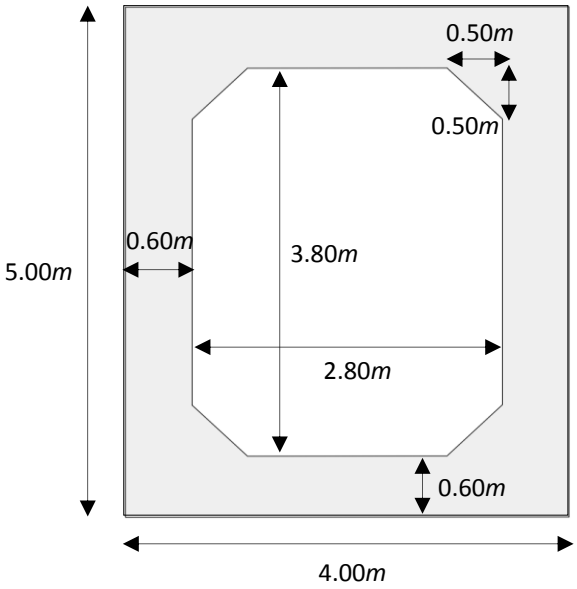

Figure 6.4: Bridge's pier section.

Table 6.7: Dynamic eigenfeatures of the initial structure.

Mass, m_s (tn)	Total Stiffness, k_o (kN/m)	Period, T (sec)	Frequency, f (Hz)	Damping Ratio, ζ (%)
2132.34	24540 (=16x2045)	1.65	0.62	5

Regarding the information provided in Section 5.2 of the current effort and following the HS optimization process, the optimum values of the KDamper design variables, required to mitigate the seismic effects in this particular bridge structure, are given in Table 6.8. The resulting values of the KDamper elements' constants are included in Table 6.9.

Table 6.8: Optimum values of the design variables.

μ	κ	ζ_D (%)
0.02	4.1	30

Table 6.9: Values of KDamper parameters and resulting values of the KDamper elements' constants.

m_D (tn)	c_D (kNs/m)	k_R (kN/m)	k_e (kN/m)	k_N (kN/m)
42.65	109.28	48982	3966.4	-3188.6

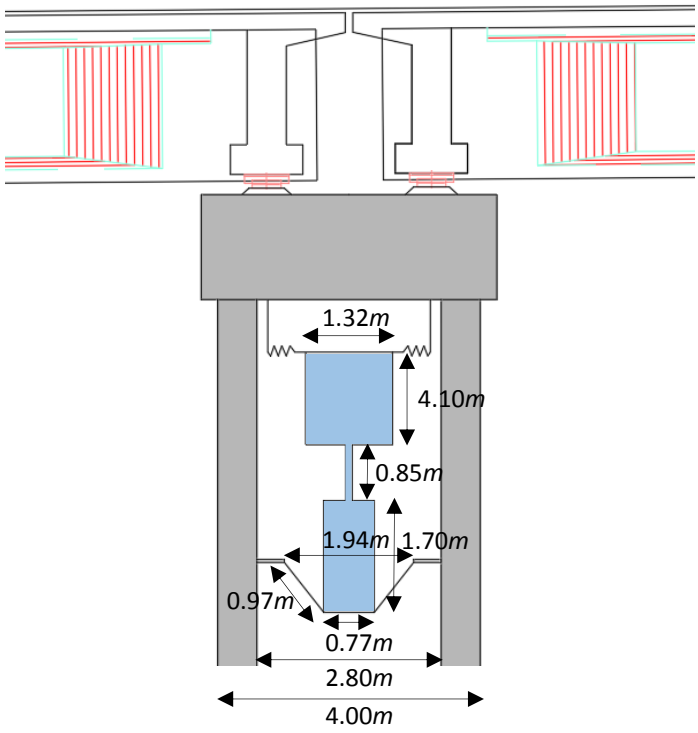

Figure 6.5: Implementation of the inverted pendulum inside the hollow pier (longitudinal section).

As long as the considered concrete bridge has hollow piers, it is hereby proposed that the inverted pendulum configuration, namely proposed configuration 2 (Section 3.3.2) is the most suitable one. Since there are two hollow piers available, two pendulums are used and, by extent, in practice, the values included in Table 6.9, concerning elements' coefficients, are divided by two. A schematic representation of the implementation of the inverted pendulum configuration inside one of the hollow piers is depicted in Fig. 6.5.

Following the steps described in Section 3.3.2, the four controlling parameters as well as the rest of the geometric dimensions of each one of the two additional masses are calculated. Their values are presented in Tables 6.10 and 6.11, respectively. In this application the material used to realize the additional mass is steel, with a value of density equal to $\rho_{mat} = 7850\ kg/m^3$.

Table 6.10: Values of four basic dimensions and relative negative stiffness of each inverted pendulum.

K_{REL}	c (m)	d (m)	l (m)	h (m)
-0.747	0.386	0.97	0.97	0.85

Table 6.11: Values of the rest dimensions of each additional mass.

V_{tot} (m^3)	d_b (m)	x_b (m)	x_u (m)	d_u (m)	R (m)
2.72	1.7	1.7	0.7	1.41	0.66

Since the free space provided inside the hollow pier is limited, after the computation of the dimensions of Tables 6.10 and 6.11, the following check has to be carried out

$$2R + 2u_D < 2.8 \tag{6.3.1}$$

where 2.8 is the free span of the hollow section in the longitudinal direction and u_D is the estimated horizontal displacement of the upper part of the inverted pendulum's mass, corresponding to the values of the KDamper elements of Tables 6.8 and 6.9. For the bridge considered, this is approximately equal to 0.70 *m* and Eq. (6.3.1) is valid.

6.3.2 Results

Table 6.12: Dynamic eigenfeatures of the KD structure in comparison with the corresponding ones of the initial structure.

	Period, T (sec)	Frequency, f (Hz)	Damping Ratio, ζ (%)
Initial Structure	1.65	0.62	5
Isolated Structure	2.35	0.43	31.9

Time history analysis is performed on both the initial and the KD system using Newmark-β time integration method. In addition, the KD system is subjected to a free vibration with initial conditions, aiming to calculate its damping ratio. The dynamic eigenfeatures of the KD structure are included in Table 6.12, in comparison with the corresponding ones of the initial structure. The results of the

dynamic response of both structures are presented in Table 6.13, in both terms of deck's relative displacement and deck's absolute acceleration.

Table 6.13: Comparative results of the dynamic response of both the initial structure and the structure with KDampers, in terms of relative deck displacement and absolute deck acceleration.

	Initial Structure		**KD Structure**		**Reduction (%)**	
	$\mathbf{u_{rel}}$ **(m)**	$\mathbf{a_{abs}}$ **(m/s^2)**	$\mathbf{u_{rel}}$ **(m)**	$\mathbf{a_{abs}}$ **(m/s^2)**	$\mathbf{u_{rel}}$	$\mathbf{a_{abs}}$
Aigio	0.21	13.67	0.14	2.96	33.3	78.3
Athens	0.19	14.06	0.11	2.62	42.1	81.4
Kalamata	0.23	8.88	0.11	2.80	52.2	68.5

Observing Table 613, the improved dynamic behavior of the KD systems is demonstrated, since a drastic reduction of both deck relative displacements and deck absolute accelerations is noticed for all three earthquakes. Precisely, and average 42.5 % reduction is estimated for the deck's relative displacements, whereas regarding the deck's absolute accelerations the average percentage raises up to 76%. This fact is, also, validated by the results of Table 6.12, as the damping ration of the KD system is approximately 6 times higher than the initial one. Finally, the frequency of the isolated system, whose control parameters have been extracted from the HS optimization procedure, results equal to 0.43 Hz (value close to the assumption of Section 4.2.3) validating once more the accuracy of the optimization process results.

6.4 NUMERICAL APPLICATION 3

6.4.1 Test case considered

A different type of numerical application is presented in this section. In view of demonstrating that the implementation of the KDamper concept is realistic and feasible for bridge structures, a typical two span concrete bridge with flexible pier, similar to the one considered in Section 6.2, is, also, considered hereby. Its longitudinal and transverse sections are shown in Fig. 6.1. The dynamic eigenfeatures of the initial SDoF system are given in Table 6.14. Since the pier is considered to be flexible, its contribution to the structure's stiffness is taken into account and two different types of KDamper devices are employed. For this specific numerical application, the proposed configuration 1 of Section 3.3.1 has been selected. Further information on this numerical application can be found in Sapountzakis et al. (2017).

Table 6.14: Dynamic characteristics and eigenfeatures of the initial SDoF system.

Mass, m_s **(tn)**	k_o **(kN/m)**	k_{pier} **(kN/m)**	**Total stiffness,** k_{tot} **(kN/m)**	**Period,** T **(s)**	**Frequency,** f **(Hz)**	**Damping factor,** c_s**, (kNs/m)**	**Damping ratio,** ζ **(%)**
723.9	13650	73344	13552.03	1.45	0.70	314.3443	5

where, k_o is the total stiffness of the elastomeric bearings, which are going to be replaced by the KDamper devices and k_{pier} is the stiffness of the middle pier.

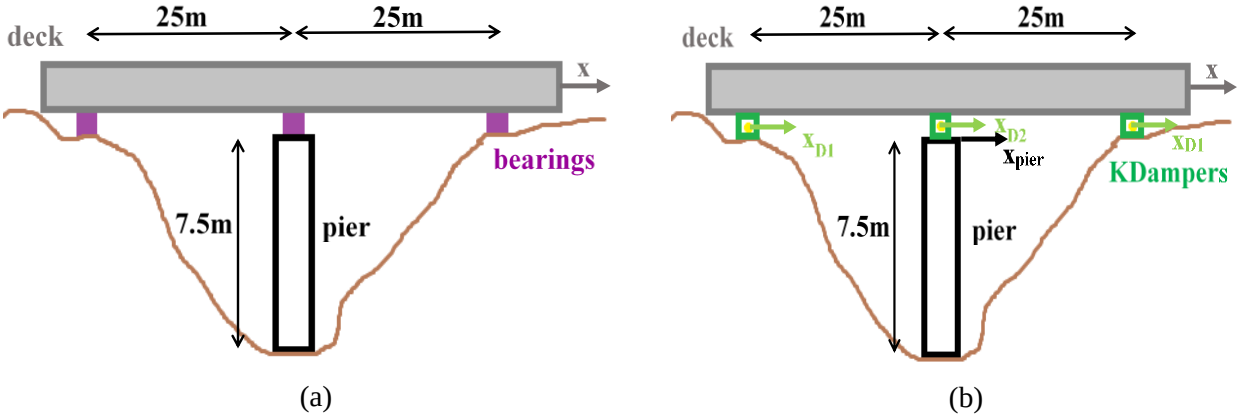

Figure 6.6: Schematic representation of the DoFs of the bridge structure (a) before (initial SDoF system) and (b) after the implementation of the KDamper devices (isolated 4DoF system).

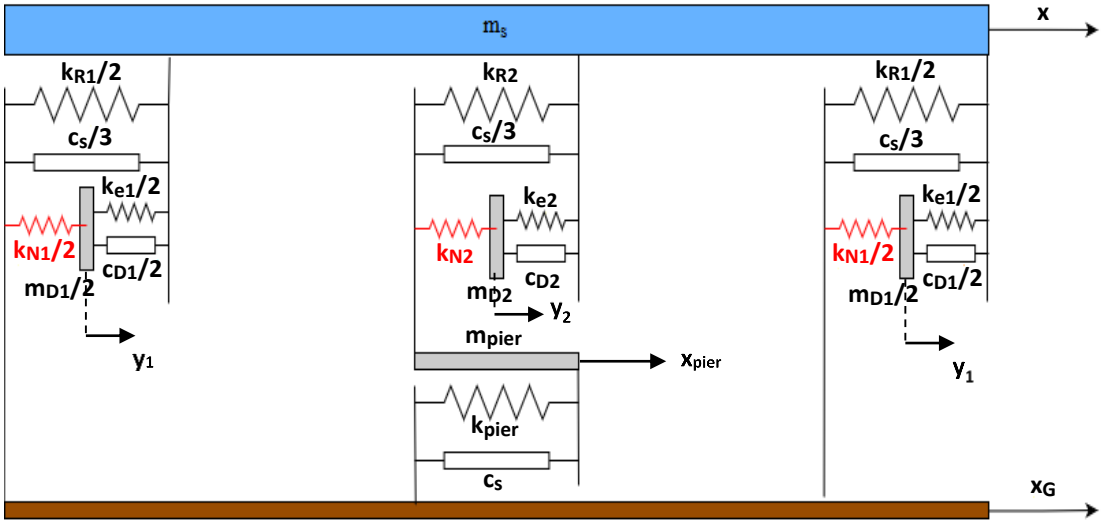

Figure 6.7: Detailed schematic representation of the isolated system after the implementation of the KDamper devices.

After the implementation of the KDamper devices, the initial SDoF system is substituted by a 4DoF system, since two types of KDamper devices are used, one above the abutments and one above the middle pier, in view of maximizing the effectiveness of the isolated system. These two types of KDamper devices are similar in form but differ in dimensions and numerical properties. A schematic representation of both the initial SDoF system and the isolated 4DoF system is given in Fig. 6.6. For the better understanding of the reader, a detailed illustration of the isolated system after the implementation of the KDamper devices is provided in Fig. 6.7. More specifically, Fig. 6.7 is practically, an extension of Fig. 4.1, demonstrating the flexibility and applicability of the concept in systems with multiple DoFs.

Due to the complexity of the resulting 4DoF system and since this application aims to prove the effectiveness of the KDamper concept for bridges with flexible piers, under different types of dynamic

loading, and not the robustness of the optimization algorithm, the device's parameters have been chosen through a trial and error procedure, in order to determine the ones that provide the structure with an enhanced dynamic performance.

The system of nonlinear (Eqs. (6.2.1)) equations for the previously described isolated 4DoF system (Fig. 6.7) is given as

$$\begin{aligned} &m_s\ddot{u}_{deck} + \left(c_s + c_{D1} + c_{D2}\right)\dot{u}_{deck} - c_{D2}\dot{u}_{D2} - c_{D1}\dot{u}_{D1} - c_s\dot{u}_{pier} + \\ &+\left(k_{R2} + k_{e2} + k_{R1} + k_{e1}\right)u_{deck} - k_{e2}u_{D2} - k_{e1}u_{D1} - k_{R2}u_{pier} = -m_s\ddot{x}_G \end{aligned} \tag{6.2.1a}$$

$$m_{D2}\ddot{u}_{D2} - c_{D2}\dot{u}_{deck} + c_{D2}\dot{u}_{D2} - k_{e2}u_{deck} + k_{e2}u_{D2} + f_{ND2} - f_{NDpier} = -m_{D2}\ddot{x}_G \tag{6.2.1b}$$

$$m_{D1}\ddot{u}_{D1} - c_{D1}\dot{u}_{deck} + c_{D1}\dot{u}_{D1} - k_{e1}u_{deck} + k_{e1}u_{D1} + f_{ND1} = -m_{D1}\ddot{x}_G \tag{6.2.1c}$$

$$\frac{1}{2}m_{pier}\ddot{u}_{pier} - c_s\dot{u}_{deck} + c_s\dot{u}_{pier} - k_{R2}u_{deck} - f_{ND2} + \left(k_{R2} + k_{pier}\right)u_{pier} + f_{NDpier} = -\frac{1}{2}m_{pier}\ddot{x}_G \tag{6.2.1d}$$

where,

$$u_{deck} = x - x_G \tag{6.2.2a}$$

$$u_{D1} = y_1 - x_G \tag{6.2.2b}$$

$$u_{D2} = y_2 - x_G \tag{6.2.2c}$$

In Eqs. (6.2.1b) – (6.2.1d), f_{ND1}, f_{ND2} and f_{NDpier} are calculated according to Eq. (3.3.3).

The 4DoF system is subjected to three different dynamic loads: (a) a seismic excitation, namely Tabas earthquake excitation record (Fig. 6.8), (b) a harmonic excitation, in resonance with the initial structure's eigenfrequency (Fig. 6.9), and (c) a step function simulating the effect of a breaking force on the bridge's deck (Fig. 6.10. Finally, a free vibration with initial conditions is carried out, in order to determine the isolated system's damping ratio. For all these cases, the system of Eqs. (6.2.1) is solved using the Newmark-β method, with linear acceleration.

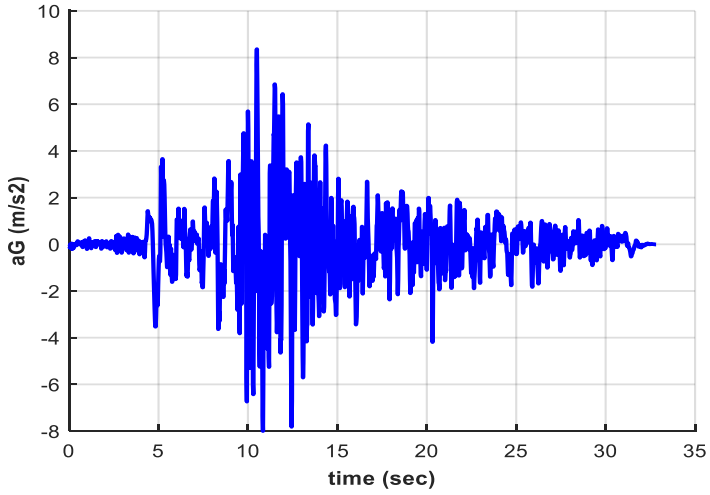

Figure 6.8: Ground acceleration excitation considered (TABAS, a_G = 8.36 m/s^2).

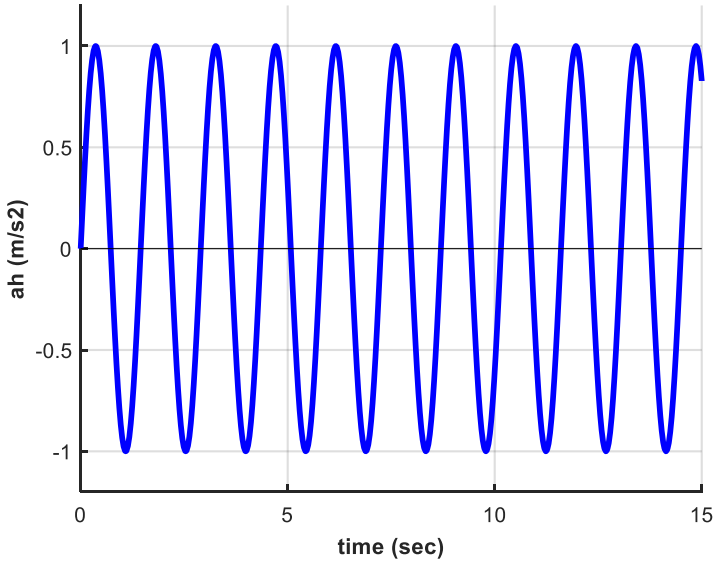

Figure 6.9: Harmonic excitation considered *(amplitude = 1,* $\omega_s = 4.33$ *rad/sec).*

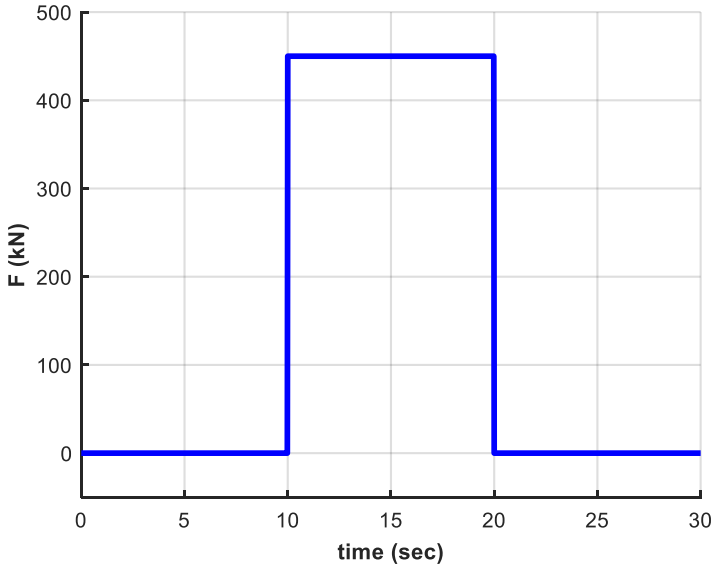

Figure 6.10: *Step function considered (for* $20 \le t \le 30\,sec,\ F_c = 450\,kN$ *).*

6.4.2 Results

The values of the KDamper elements coefficients and of its basic parameters are included in Table 6.15. The values of the proposed configuration 1 parameters, which was employed for this numerical application, are given in Table 6.16. The dynamic eigenfeatures of both the initial and the isolated systems are given in Table 6.17, whereas comparative results between the two aforementioned systems for each one of the three earthquake excitations can be found in Table 6.6, in terms of the deck's absolute acceleration and relative displacement. The corresponding comparative, between the initial SDoF and the isolated 4DoF structure, time history results, for the three aforementioned loadings are provided in Figs. 6.11, 6.12 and 6.13, respectively. An overall improved dynamic behavior is demonstrated in all kinds of dynamic loads.

Table 6.15: Full set of parameters for each one of the nine KDampers ($i=1$ corresponds to each one of the eight KDampers above the abutments, whereas $i=2$ corresponds to the KDamper above the middle pier).

	μ_i	κ_i	ρ_i	ε_i	ζ_{Di}	k_{Ri} (kN/m)	k_{ei} (kN/m)	k_{Ni} (kN/m)	m_{Di} (tn)	c_{Di} (kNs/m)
$i=1$	0.04	3.95	1.1695	0.108	0.724	2825.3	369.7	-295	3.62	23.4
$i=2$	0.01	4.55	1.0615	0.163	0.350	1506.8	170.7	-140	7.24	11.6

Table 6.16: Negative stiffness spring and mechanism parameters for each one of the nine KDampers ($i=1$ corresponds to each one of the eight KDampers above the abutments, whereas $i=2$ corresponds to the KDamper above the middle pier).

	k_{Hi} (kN/m)	l_{HIi} (m)	a_i (m)	b_i (m)	u_{oi} (m)
$i=1$	156.82	1.297	0.65	1.330	0.005
$i=2$	74.40	1.360	0.70	1.395	0.005

Table 6.17: Dynamic eigenfeatures of the KD structure in comparison with the corresponding ones of the initial structure.

	Period, *T* (sec)	**Frequency, *f* (Hz)**	**Damping Ratio, ζ (%)**
Initial Structure	1.45	0.70	5
Isolated Structure	2.94	0.34	11.4

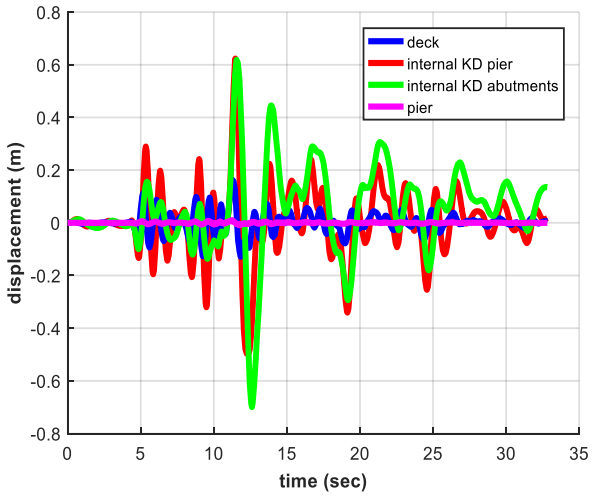

(a)

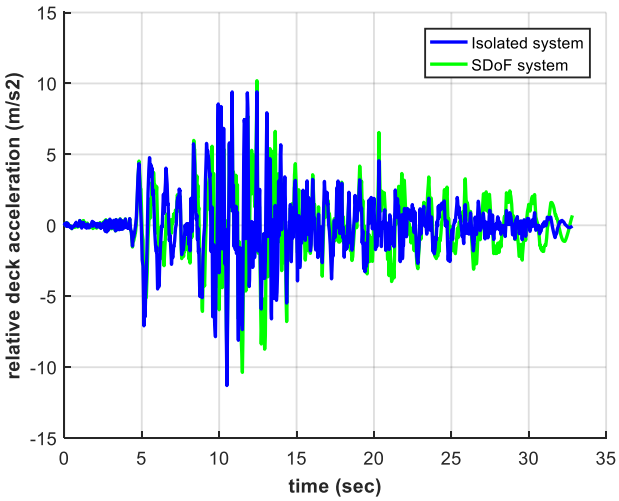

(b)

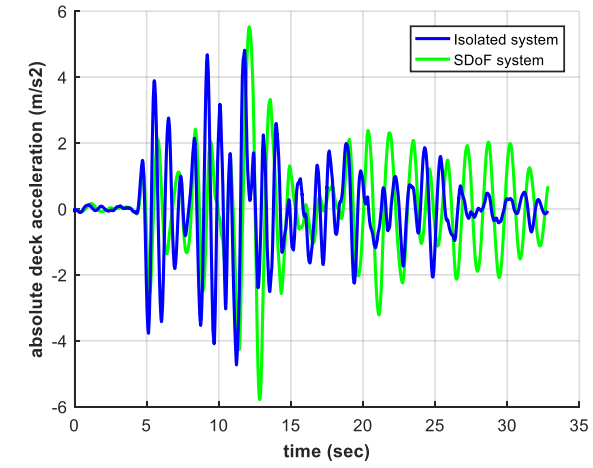

(c)

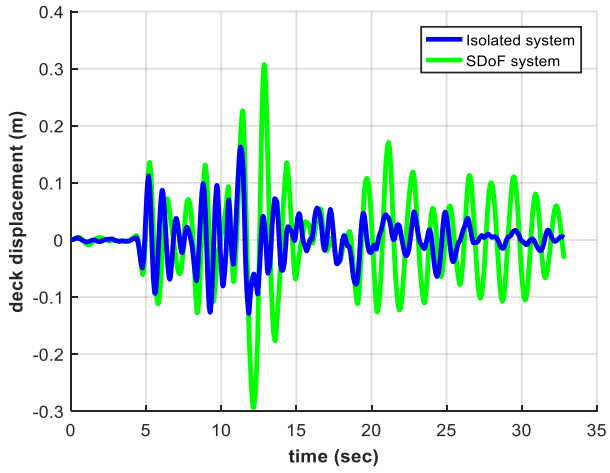

(d)

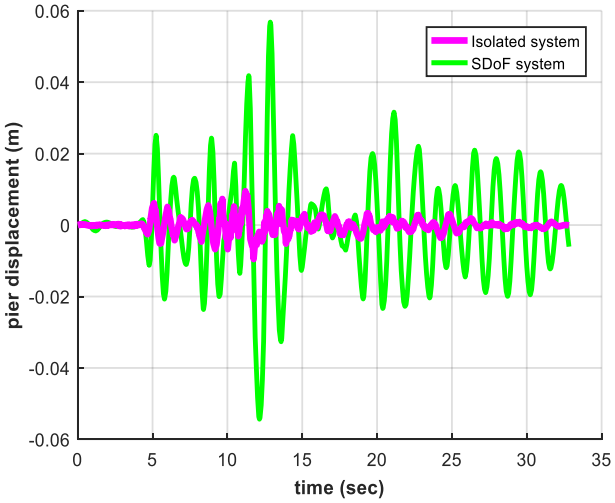

(e)

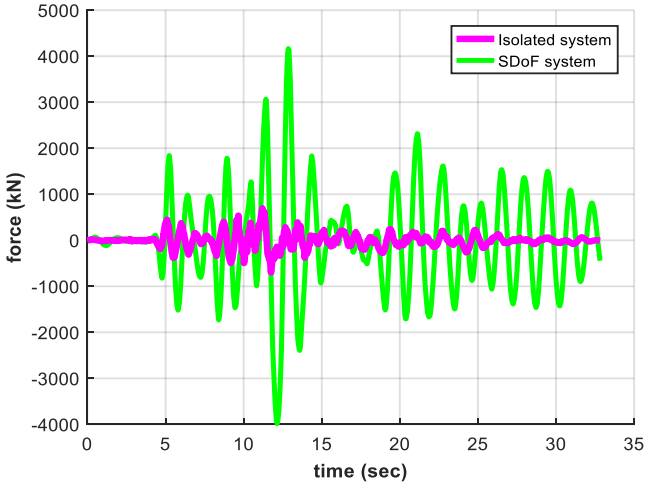

(f)

Figure 6.11: (a) Dynamic response of the isolated non-linear system for all four DoFs - displacements in *m* ($\max|u_{deck}|=0.16, \max|u_{D1}|=0.70, \max|u_{D2}|=0.62, \max|u_{pier}|=0.010$) and comparative results between the initial and the isolated system (b) deck's relative acceleration in *m/s*^{2} ($\max|a_{KD}|=11.29$, $\max|a_{SDoF}|=10.37$), (c) deck's absolute acceleration in *m/s*^{2} ($\max|a_{KD}|=4.81, \max|a_{SDoF}|=5.79$), (d) deck's displacements in *m* ($\max|u_{KD}|=0.16, \max|u_{SDoF}|=0.31$), (e) displacements on the top of the pier in *m* ($\max|u_{KD}|=0.010, \max|u_{SDoF}|=0.060$), (f) forces at the top of the middle pier in *kN* ($\max|F_{KD}|=698.50, \max|F_{SDoF}|=4165.72$).

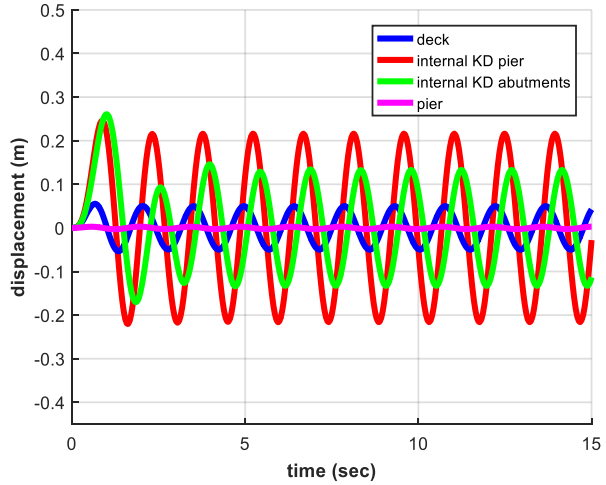

(a)

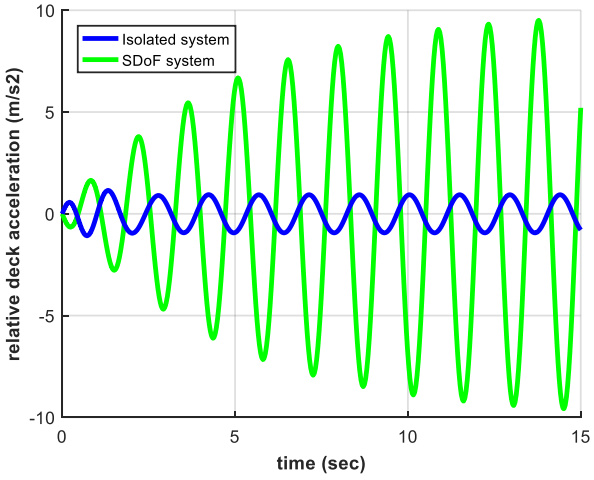

(b)

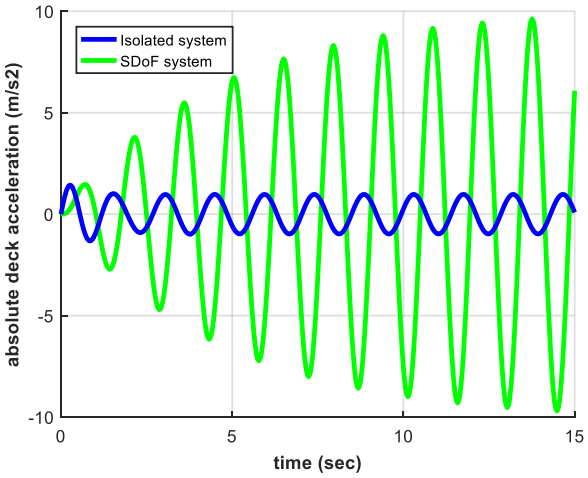

(c)

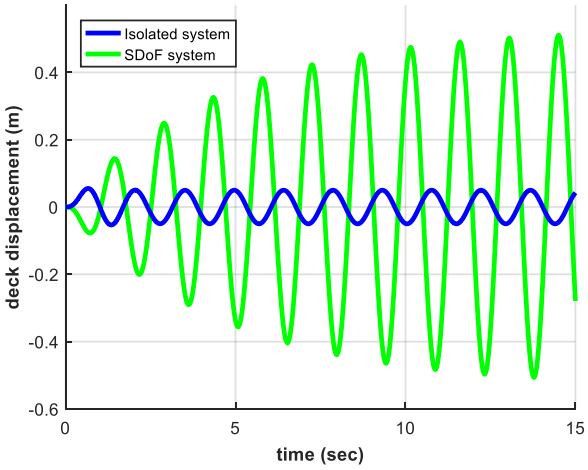

(d)

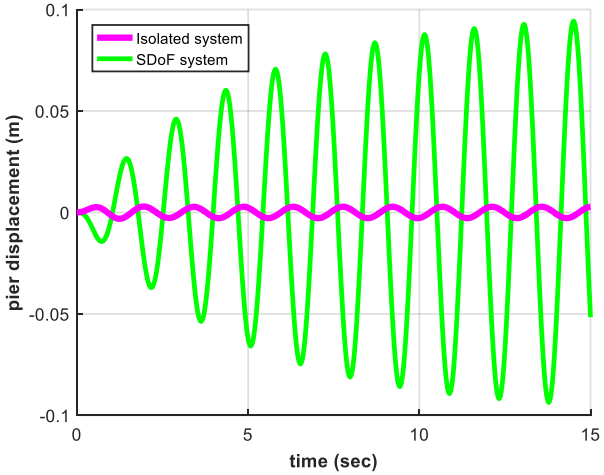

(e)

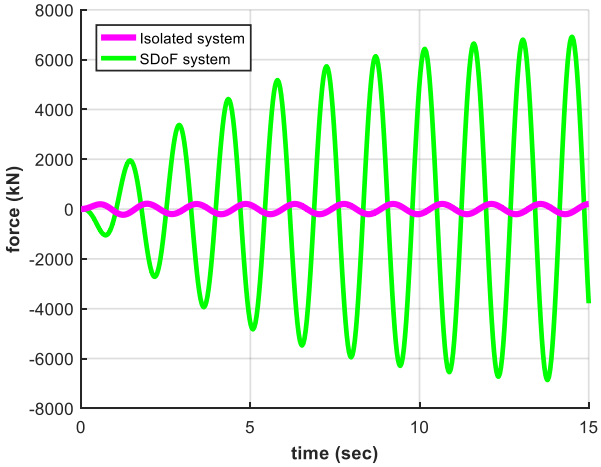

(f)

Figure 6.12: (a) Dynamic response of the isolated non-linear system for all four DoFs - displacements in m ($\max|u_{deck}| = 0.06$, $\max|u_{D1}| = 0.26$, $\max|u_{D2}| = 0.25$, $\max|u_{pier}| = 0.003$) and

comparative results between the initial and the isolated system (b) deck's relative acceleration in m/s^2 ($\max|a_{KD}|=1.15$, $\max|a_{SDoF}|=9.58$), (c) deck's absolute acceleration in m/s^2 ($\max|a_{KD}|=1.43$, $\max|a_{SDoF}|=9.70$), (d) deck's displacements in m ($\max|u_{KD}|=0.06$, $\max|u_{SDoF}|=0.51$), (e) displacements on the top of the pier in m ($\max|u_{KD}|=0.003$, $\max|u_{SDoF}|=0.090$), (f) forces at the top of the middle pier in kN ($\max|F_{KD}|=229.14$, $\max|F_{SDoF}|=6918.83$).

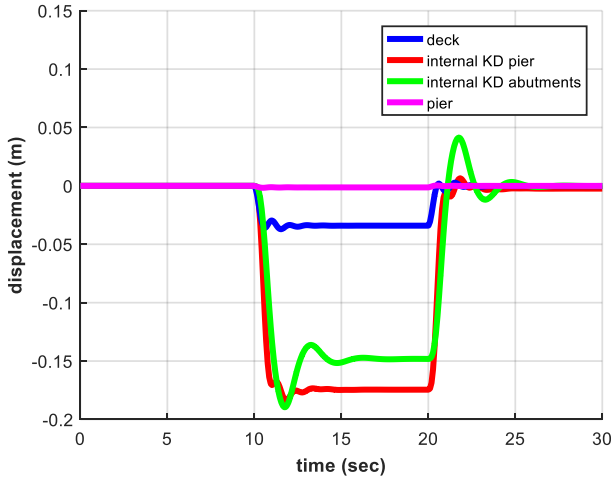

(a)

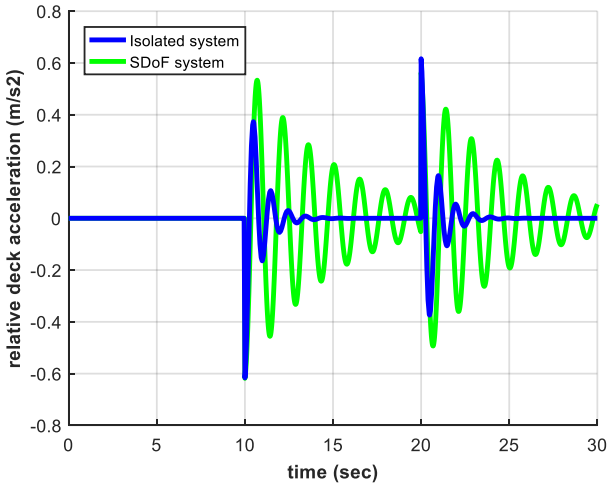

(b)

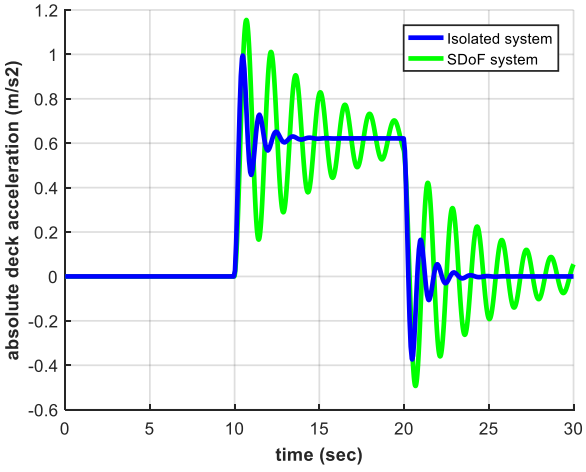

(c)

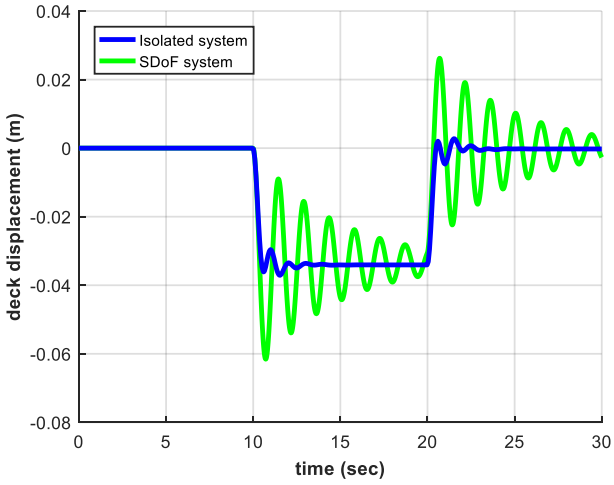

(d)

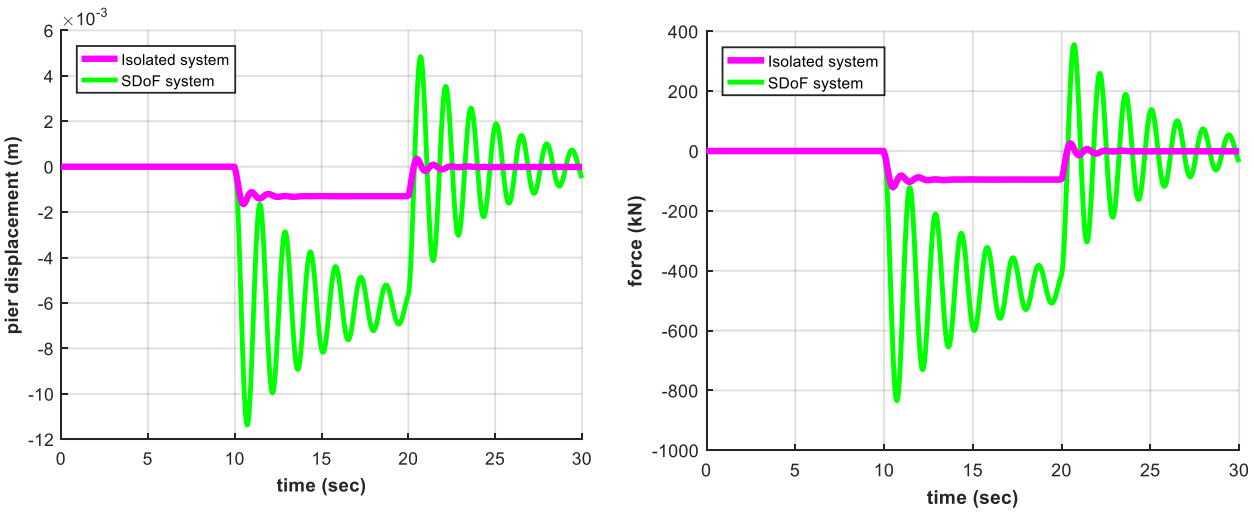

(e) (f)

Figure 6.13: (a) Dynamic response of the isolated non-linear system for all four DoFs - displacements in m ($\max|u_{deck}| = 0.04$, $\max|u_{D1}| = 0.19$, $\max|u_{D2}| = 0.18$, $\max|u_{pier}| = 0.002$) and comparative results between the initial and the isolated system. (b) deck's relative acceleration in m/s^2 ($\max|a_{KD}| = 0.62$, $\max|a_{SDoF}| = 0.62$), (c) deck's absolute acceleration in m/s^2 ($\max|a_{KD}| = 0.99$, $\max|a_{SDoF}| = 1.16$), (d) deck's displacements in m ($\max|u_{KD}| = 0.036$, $\max|u_{SDoF}| = 0.06$), (e) displacements on the top of the pier in m ($\max|u_{KD}| = 0.002$, $\max|u_{SDoF}| = 0.01$), (f) forces at the top of the middle pier in kN ($\max|F_{KD}| = 121.02$, $\max|F_{SDoF}| = 834.36$).

Observing Figs. 6.11e, 6.11f, 6.12e, 6.12f, 6.13e and 6.13f, regarding the forces and displacements at the top of the bridge's pier, it can be extracted that a more economic design can be achieved for the pier, since the dynamic demands are significantly reduced.

Conclusions

Summarizing all the information included in the previous Chapters of this Master Thesis, entitled "Design and Optimization of Systems with Negative Stiffness Elements for Bridge Seismic Isolation", the following remarks can be made:

- Seismic isolation is a contemporary technique, offering earthquake effects mitigation to structures.
- Numerous seismic isolation devices, mechanisms and configurations have already been invented, tested and applied on real structures and, especially, on bridge structures. Bearings are a characteristic example, along with other more complex configurations such as the TMDs.
- Negative stiffness elements exhibit unique properties by enabling period shift and, simultaneously, absorbing energy, when incorporated to a structure.
- The KDamper concept is based on the combination of the positive features of TMDs and negative stiffness elements, without their drawbacks.
- The KDamper concept is applicable not only on bridges, but, also, in other types of structures. For instance, tall building or industrial facilities.
- Metaheuristic algorithms simulate natural phenomena. They are suitable for numerous complex mathematical and engineering optimization problems. Harmony Search algorithm is one of them, that differs, since it is based on the use of stochastic derivatives.
- The design and optimization procedure of the KDamper concept depends on the type of bridge to which it will be implemented, on which mechanical configuration will be employed, on the mechanical equipment and on the physical and manufacturing constraints that might be imposed. However, it is an overall straightforward procedure and only small alterations are required to adjust.

- Three different numerical applications of the KDamper on bridge structures validate, not only the accuracy and efficiency of the proposed seismic effects mitigation method, but, also, the robustness of the HS optimization algorithm.
- Observing the results obtained for all three numerical applications, it can be noticed that at all cases, the resulting isolated structure (after the implementation of the KDamper devices) demonstrates an overall improved dynamic performance, in both terms of accelerations and displacements.
- The enhanced dynamic performance is observed in all kinds of dynamic loads, even under high frequency seismic excitations, as the numerical application 3 proves.
- The achieved damping ratio for all isolated systems is more than 2 times larger than the corresponding ratio of the original structure.
- The proposed configuration 2 – inverted pendulum is the most suitable when dealing with bridges whose piers have a hollow cross section.
- A relatively small additional mass is required, especially, at the case of numerical application 2. This fact, along with the absence of detuning phenomena, renders the KDamper concept a competitive alternative against TMDs.

Appendix A: Calculation of coefficients C_ρ and B_ρ of Equation (4.2.8)

A.1 CALCULATION OF COEFFICIENTS C_ρ AND B_ρ FOR ESTIMATING PARAMETER ρ

In this appendix, the calculation of coefficients C_ρ and B_ρ required to estimate the value of the parameter ρ is presented. The two aforementioned coefficients are computed according to Eqs. (A.1).

$$B_{\rho A} = \left[\left(A_{0\rho}D_{20} + D_{2\rho}A_{00}\right) + \left(A_{2\rho}D_{00} + D_{0\rho}A_{20}\right) + \left(B_{0\rho}C_{20} + C_{2\rho}B_{00}\right)\right]D_{20} \tag{A.1a}$$

$$B_{\rho B} = -2\left(A_{2\rho}D_{20} + A_{20}D_{2\rho} + B_{0\rho}\right)D_{00} - 2\left(A_{20}D_{20} + B_{00}\right)D_{0\rho} \tag{A.1b}$$

$$B_\rho = B_{\rho A} + B_{\rho B} \tag{A.1c}$$

$$C\rho = \left(A_{00}D_{20} + A_{20}D_{00} + B_{00}C_{20}\right)D_{20} - 2\left(A_{20}D_{20} + B_{00}\right)D_{00} \tag{A.1d}$$

where, $A_{0\rho}$, D_{20}, $D_{2\rho}$, A_{00}, $A_{2\rho}$, D_{00}, $D_{0\rho}$, A_{20}, $B_{0\rho}$, C_{20}, $C_{2\rho}$ and B_{00} are derived from Table A.1

Table A.1: Values of coefficients A_{ri}, B_{ri}, C_{ri} and D_{ri} for $r = 2\,or\,0$.

	A2i	**A0i**	**B0i**	**C2i**	**C0i**	**D2i**	**D0i**
$i = \rho$	0	$1+(1+\kappa)\mu$	0	$-\left[1+(1+\kappa)^2\mu\right]$	0	0	$\kappa^2\mu$
$i = 0$	-1	0	$1+\mu$	-1	1	$-(1+\mu)$	1

After successive substitution of the coefficients of Table A.1 into Eqs. (A.1) and of Eqs. (A.1c) and (A.1d) into Eq. (4.2.8), the following relation is obtained:

$$\rho(\kappa,\mu) = \sqrt{\frac{1}{(1+\mu+\kappa\mu)(1+\mu)-\kappa^2\mu}} \tag{A.2}$$

namely, Eq. (4.2.9), giving the value of the parameter ρ for each set of the parameters μ and κ.

Appendix B: Derivation of Equations (4.2.10a) - (4.2.10c)

B.1 CONCISE DERIVATION OF EQUATIONS (4.2.10A) - (4.2.10C)

In this appendix, the concise derivation of Eqs. (4.2.10a-4.2.10c) is presented. Precisely, the following steps are followed:

Starting from Eq. (4.2.4b),

$$\kappa = -\frac{k_N}{k_e + k_N} \Rightarrow k_N = -\kappa\left(k_e + k_N\right) \tag{B.1}$$

$$\frac{k_N}{k_o} = -\kappa\frac{k_e + k_N}{k_o} \tag{B.2}$$

From Eqs. (4.2.7) and considering that $k_D = k_e + k_N$, the following relations can be derived

$$k_e + k_N = m_D\omega_D^2 \tag{B.3a}$$

$$k_o = m_s\omega_s^2 \tag{B.3b}$$

After substituting Eqs. (B.3) to Eq. (B.2), the latter becomes

$$\frac{k_N}{k_o} = -\kappa\frac{m_D\omega_D^2}{m_s\omega_s^2} \Rightarrow \frac{k_N}{k_o} = -\kappa\frac{m_D}{m_s}\left(\frac{\omega_D}{\omega_s}\right)^2 \tag{B.4}$$

Taking into account Eqs. (4.2.4a) and (4.2.6), Eq. (B.4) becomes

$$\frac{k_N}{k_o} = -\kappa\mu\rho^2 \tag{B.5}$$

namely, Eq. (4.2.10a).

Following the first two steps the previously described procedure, Eq. (B.6) is derived

$$\frac{k_e + k_N}{k_o} = -\frac{1}{\kappa}\frac{k_N}{k_o} \Rightarrow \frac{k_e}{k_o} + \frac{k_N}{k_o} = -\frac{1}{\kappa}\frac{k_N}{k_o} \Rightarrow \frac{k_e}{k_o} = -\frac{1}{\kappa}\frac{k_N}{k_o} - \frac{k_N}{k_o} \tag{B.6}$$

and after substituting Eqn. (A5)

$$\frac{k_e}{k_o} = -\frac{1}{\kappa}\left(-\kappa\mu\rho^2\right) - \left(-\kappa\mu\rho^2\right) \Rightarrow \frac{k_e}{k_o} = \mu\rho^2 + \kappa\mu\rho^2 \tag{B.7}$$

leading after manipulations to

$$\frac{k_e}{k_o} = \left(1 + \kappa\right)\mu\rho^2 \tag{B.8}$$

namely, Eq. (4.2.10b).

Finally, combining Eqs. (4.2.1) and (4.2.4b), the stiffness coefficient k_R is given by

$$k_R = k_o + \kappa k_e \tag{B.9}$$

Dividing by k_o Eq. (B.9) becomes

$$\frac{k_R}{k_o} = 1 + \kappa \frac{k_e}{k_o} \tag{B.10}$$

which after substituting Eq. (B.8) gives

$$\frac{k_R}{k_o} = 1 + \kappa (1 + \kappa) \mu \rho^2 \tag{B.11}$$

namely, Eq. (4.2.10c).

References

(in alphabetical and chronological order)

Ahmadi, G. (1983), "*Stochastic Earthquake Response of Structures on Sliding Foundation*", International Journal of Engineering Science, **21**, 2, 93-102.

Antoniadis, I., Chronopoulos, D., Spitas, V. and Koulocheris, D. (2015), "*Hyper-damping properties of a stable linear oscillator with a negative stiffness element*". Journal of Sound and Vibration, **346**, 37-52.

Antoniadis, I.A., Kanarachos, S.A., Gryllias, K. and Sapountzakis, I.E. (2016), "*KDamping: A stiffness based vibration absorption concept*". Journal of Vibration and Control, DOI: 10.1177/1077546316646514.

Attary, N., Symans, M., Nagarajaiah, S., Reinhorn, A.M., Constantinou, M.C., Taylor, D., Sarlis, A.A. and Pasala, D.T.R. (2012b), "*Application of Negative Stiffness Devices for Seismic Protection of Bridge Structures*". Proc. of ASCE Structures Congress, Chicago, March.

Attary, N., Symans, M., Nagarajaiah, S., Reinhorn, A.M., Constantinou, M.C., Taylor, D., Pasala, D.T.R. and Sarlis, A.A. (2012b), "*Performance Evaluation of a Seismically-isolated Bridge Structure with Adaptive Passive Negative Stiffness*". 15th World Conference on Earthquake Engineering, Lisbon, Portugal, September.

Attary, N., Symans, M. and Nagarajaiah, S. (2015), "*Development of a rotation-based negative stiffness device for seismic protection of structures*". Journal of Vibration and Control, DOI: 10.1177/1077546315585435.

Baravelli, E. and Ruzzene, M. (2013), "*Internally resonating lattices for bandgap generation and low-frequency vibration control*". Journal of Sound and Vibration **332**: 6562–6579.

Bednarski, E. J. (1935), Discussion of Paper No. 1906, "*Flexible 'First-Story' Construction for Earthquake Resistance*", 7hansactions A.S.C.E., **100**, 657-660.

Buckle, I.G. and Mayes, R.L. (1990), "*Seismic Isolation: History, Application and Performance – A World View*". Earthquake Spectra, **6**, 161-201.

Calantarients, J.A. (1909), "*Improvements in and Connected with Building and Other Works and Appurtenances to Resist the Action of Earthquakes and the Like*", Paper No. 325371, Engineering Library, Stanford University, Stanford, California.

Carella, A., Brennan, M. and Waters, T. (2007), "*Static analysis of passive vibration isolator with quasi-zero-stiffness characteristic*". Journal of Sound and Vibration, **301**, 678-689.

Caspe, M. S. (1970), "*Earthquake Isolation of Multi-Storey Concrete Structures*", Journal of the American Concrete Institute, **11**, 923-933.

Caspe, M. S. (1984), "*Base Isolation from Earthquake Hazards, an Idea Whose Time Has Come!*", 8th World Conference on Earthquake Engineering, San Francisco, **5**, 1031-1038.

Constantinou, M.C., Kalpakidis, I., Filiatrault, A. and Ecker Lay, R.A. (2011), "*LRFD-Based Analysis* and Design Procedures for Bridge Bearings and Seismic Isolators". MCEER, Technical Report.

Correa, D.M., Klatt, T., Cortes, S., et al. (2015), "*Negative stiffness honeycombs for recoverable shock isolation*". Rapid Prototyping Journal **21**, 193–200.

Debnath N., Deb S.K. and Dutta A. (2015), "*Multi-modal vibration control of truss bridges with tuned mass dampers under general loading*". Journal of Vibration and Control, DOI: 10.1177/1077546315571172.

Den Hartog J.P. (1956), Mechanical Vibrations. 4th ed. New York: McGraw-Hill.

DeSalvo, R. (2007), "*Passive, nonlinear, mechanical structures for seismic attenuation*". Journal of Computational and Nonlinear Dynamics, **2**, 290-298.

Dong, L. and Lakes, R. (2013), "*Advanced damper with high stiffness and high hysteresis damping based on negative structural stiffness*". International Journal of Solids and Structures **50**, 2416–2423.

Dyskin, A.V. and Pasternak, E. (2012), "*Mechanical effect of rotating non-spherical particles on failure in compression*". Philosophical Magazine **92**, 3451–3473.

Erdal, F. and Saka, M.P. (2009), "*Harmony search based algorithm for the optimum design of grillage systems to LFRD-AISC*". Structural and Multidisciplinary Optimization, **38**, 25-41.

Fintel, M. and Khan, R. F. (1969), "*Shock Absorbing Soft Story Concept for Multistory Earthquake Structures*", Journal of the American Concrete Institute, 66-29, 318-390.

Frahm H. (1909), Device for Damping Vibrations of Bodies. US patent #989958.

Gao, X.Z., Govindasamy, V., Xu, H., Wang, X., Zenger, K. (2015), "*Harmony search method: Theory and applications*". Computational Intelligence and Neuroscience, **2015**, 1-10.

Geem, Z.W., Kim, J.H. and Loganathan, G.V. (2001), "*A new heuristic optimization algorithm: harmony search*". Simulation, **76**, 60-68.

Geem, Z.W., Kim, J.H. and Loganathan, G.V. (2002), "*Harmony search optimization: Application to pipe network design*". International Journal of Modelling and Simulation, **22**, 125-133.

Geem, Z.W., Tseng, C. and Park, Y. (2005), "*Harmony search for generalized orienteering problem: Best touring in China*". Springer Lecture Notes in Computer Science, **3412**, 741-750.

Geem, Z.W. (2008), "*Novel derivative of harmony search algorithm for discrete design variables*". Applied Mathematics and Computation, **199**, 223-230.

Glover, F. (1977), "*Heuristic for Integer Programming Using Surrogate Constraints*". Decision Sciences, **8** (1), 156-166.

Goldberg, D.E. (1989), "*Genetic Algorithms in Search Optimization and Machine Learning*". Addison Wesley.

Green, N. B. (1935), "*Flexible 'First-Storey' Construction for Earthquake Resistance*", Transactions A.S.C.E., **100**, Paper No. 1906, 6444-574.

Haskett T., Breukelman B., Robinson J. and Kottelenberg J. (2003), "*Tuned mass dampers under excessive structural excitation*". Report of the Motioneering Inc. Guelph, Ontario, Canada NIK 1B8.

Holland, J.H. (1975), "*Adaptation in Natural and Artificial Systems*". University of Michigan Press, Ann Arbor.

Housner, G.W. (1963), "*The behaviour of inverted pendulum structures during earthquakes*". Bulletin of the Seismological Society of America, **53** (2), 404–417.

Huffman, G. (1980), "*Spring-Damper Systems for the Support of Structures to Prevent Earthquake Damage*", Proceedings 7th World Conference on Earthquake Engineering, Istanbul, Turkey, p. 167.

Jacobsen, L. S. (1938), "*Effects of a Flexible First Story in a Building Located on Vibrating Ground*", S. 7~moshenko, 60th Anniversary Vol. Macmillan Co., New York, 93-103.

Ibrahim, R. (2008), "*Recent advances in nonlinear passive vibration isolators*". Journal of Sound and Vibration, **314**, 371-452.

Iemura, H. and Pradono, M.H. (2009), "*Advances in the development of pseudo-negative stiffness dampers for seismic response control*". Structural Control and Health Monitoring, **16**, 784-799.

Kapasakalis, K., Sapountzakis, E.J. and Antoniadis, I. (2017), "*Implementation of the KDamper concept to wind turbine towers*". Proceedings of the 6th International Conference on Computational Methods in Structural Dynamics and Earthquake Engineering, 15-17 June, Rhodes Island, Greece.

Kelly, J.M. (1986), "*Aseismic base isolation: review and bibliography*". Soil Dynamics and Earthquake Engineering, **5**, 202-216.

Kelly, J.M. and Beucke, K.E. (1983), "*A Friction Damped Base Isolation System with Fail-Safe Characteristics*", Earthquake Engineering and Structural Dynamics, **11**, 33-56.

Kelly, J.M. and Hodder, S.B. (1982), "*Experimental Study of Lead and Elastomeric Dampers for Base Isolation Systems in Laminated Neoprene Bearings*", Bulletin of the New Zealand National Society for Earthquake Engineering, **15**, 2, 53-67.

Kirkpatrick, S., Gelatt, C. and Vecchi, M. (1983), "*Optimization by Simulated Annealing*". Science, **220** (4598), 671-680.

Lakes, R. (2001), "*Extreme damping in composite materials with a negative stiffness phase*". Physical Review Letters **86**, 2897–2898.

Le, T.D. and Ahn, K.K. (2011), "*A vibration isolation system in low frequency excitation region using negative stiffness structure for vehicle seat*". Journal of Sound and Vibration **330**, 6311–6335.

Lee, C.M., Goverdovskiy, V. and Temnikov, A. (2007), "*Design of springs with negative stiffness to improve vehicle driver vibration isolation*". Journal of Sound and Vibration **302**, 865–874.

Lee, C.M. and Goverdovskiy, V. (2012), "*A multi-stage highspeed railroad vibration isolation system with negative stiffness*". Journal of Sound and Vibration **331**, 914–921.

Lee, D.M. (1980), "*Base Isolation for Torsion Reduction in Asymmetric Structures under Earthquake Loading*", Earthquake Engineering and Structural Dynamics, **8**, 349-359.

Lee, D. M. and Medland, I. C. (1978 -1), "*Base Isolation - An Historical Development, and the Influence of High Mode Responses*", Bulletin of the New Zealand National Society for Earthquake Engineering, **11**, 4, 219-233.

Lee, D. M. and Medland, I. C. (1978-2), "*Estimation of Base Isolated Structure Responses*", Bulletin of the New Zealand National Society for Earthquake Engineering, **11**, 234-244.

Lee, K.S. and Geem, Z.W. (2004), "A new structural optimization method based on the harmony search algorithm". Computers and Structures, **82**, 781-798.

Lee, K.S. and Geem, Z.W. (2005), "*A new meta-heuristic algorithm for continuous engineering optimization: Harmony search theory and practice*". Computer Methods in Applied Mechanics and Engineering, **194**, 3902-3933.

Lee, K.S., Geem, Z.W., Lee, S.H. and Bae, K.W. (2005), "*The harmony search heuristic algorithm for discrete structural optimization*". Engineering Optimization, **37**, 663-684.

Luft R.W. (1977), "*Optimal tuned mass dampers for buildings*". Journal of the Structural Division, ASCE, **103**, 1985-98.

Martel, R.R. (1929), "*The Effects of Earthquake on Buildings with a Flexible First Storey*", Bulletin of the Seismological Society of America, **19**, 3, 167-178.

McNamara R.J. (1979), "*Tuned mass dampers for buildings*". Journal of the Structural Division, ASCE, **105**, 2766-72.

Michelis, P. and Spitas, V. (2010), "*Numerical and experimental analysis of a tri-angular auxetic core made of cfr-peek using the directionally reinforced integrated single-yarn (DIRIS) architecture*". Composites Science and Technology **70**, 1064–1071.

Molyneaux, W. (1957), Supports for vibration isolation. ARC/CR-322, Aer Res Council, G. Britain.

Mostaghel, N., Hejazi, M. and Tanbakuchi, J.T. (1982-1983), "Response of Sliding Structures to Harmonic Support Motion", Report No. UTEC-82-040, University of Utah, Department of Civil Engineering, Salt Lake City, Utah, 1982. Also printed in Earthquake Engineering and Structural Dynamics, 11,355-366, 1983.

Nagarajaiah, S., Reinhorn, A.M., Constantinou, M.C., Taylor, D., Pasala, D.T.R. and Sarlis, A.A., (2010), "*Adaptive negative Stiffness: A New Structural Modification Approach for Seismic Protection*". 5th World Conference on Structural Control and Monitoring (WCSCM 2010), p. no. 103.

Nazin, V.V. (1978), "*Buildings on Gravitational Seismoisolation System in Sevastopol*", 6th Symposium on Earthquake Engineering, University of Roorkee, India, **1**, 356-368.

Nigdeli, S.M., Bekdas, G. and Alhan, C. (2014), "*Optimization of seismic isolation systems via harmony search*". Engineering Optimization, **46**, 1553-1569.

Nigdeli, S.M. and Bekdas, G. (2017), "*Optimum tuned mass damper design in frequency domain for structures*". KSCE Journal of Civil Engineering, **21**, 912-922.

Panagopoulos, V-E. (2017), "*Implementation of dampers based on inverted unstable pendulum for the seismic protection of structures*". Diploma Thesis, School of Mechanical Engineering, National Technical University of Athens, Greece, http://dspace.lib.ntua.gr/handle/123456789/45660

Pasala, D.T.R., Sarlis, A.A., Nagarajaiah, S., Reinhorn, A.M., Constantinou, M.C. and Taylor, D. (2012), "*Negative Stiffness Device for Seismic protection of Multistory Structures*". Proc. of ASCE Structures Congress, Chicago, March.

Platus, D.L. (1992), "*Negative-stiffness-mechanism vibration isolation systems*". Proc. SPIE 1619, Vibration Control in Microelectronics, Optics, and Metrology, 44 (February 1, 1992); doi:10.1117/12.56823.

Qin L., Yan W. and Li Y. (2009), "*Design of frictional pendulum TMD and its wind control effectiveness*". Earthquake Engineering and Engineering Vibrations, **29**, 153-7.

Robertson, S., Kidner, M.R.F., Cazzolato, B.S., et al. (2009), "*Theoretical design parameters for a quasi-zero stiffness magnetic spring for vibration isolation*". Journal of Sound and Vibration **326**, 88–103.

Robinson, W. H. and Tucker, A. G. (1977), "*A Lead-Rubber Shear Damper*", Bulletin of the New Zealand National Society for Earthquake Engineering, **10**, 3, 151-153.

Ryuiti, O. (1941), "*Experiment on Earthquake Construction using Roller Type Damper*", Journal of Architectural Institute of Japan, **32**.

Ryuiti, O. A (1951), "*Note on the Seismofree Foundation*", Journal of Architectural Institute of Japan, **42**.

Ryuiti, O. A (1952), "*Study of the Seismofree Building Structures*", Journal of Architectural Institute of Japan, **43**.

Ryuiti, O. (1956), "*Practical Use of Seismofree Foundation*", Journal of Architectural Institute of Japan, **47**.

Saka, M.P. (2009), "*Optimum design of steel sway frames to BS5950 using harmony search algorithm*". Journal of Constructional Steel Research, **65**, 36-43.

Sapountzakis, E.J., Syrimi, P.G., Pantazis, I.A. and Antoniadis, I.A, (2016), "*KDamper Concept in Seismic Isolation of Bridges*". Proc. of the 1th International Conference on Natural Hazards and Infrastructure (ICONHIC 2016), Chania, Crete, Greece, June 28-30.

Sapountzakis, E.J., Syrimi, P.G., Pantazis, I.A. and Antoniadis, I.A, (2017), "*KDamper Concept in Seismic Isolation of Bridges with Flexible Piers*". Engineering Structures, **153**, 525-539.

Sarlis, A.A., Pasala, D.T.R., Constantinou, M.C., Reinhorn, A.M., Nagarajaiah, S. and Taylor, D. (2011), "*Negative Stiffness Device for Seismic Protection of Structures – An Analytical and Experimental Study*". 3th International Conference on Computational Methods in Structural Dynamics and Earthquake Engineering (COMPDYN 2011), Corfu, Greece, May 26-28.

Sarlis, A.A., Pasala, D.T.R., Reinhorn, A.M., Constantinou, M.C., Nagarajaiah, S. and Taylor, D. (2012), "*Negative stiffness device for seismic protection of structures*". Journal of Structural Engineering, **139**, 1124-1133.

Seismosoft (2016) "SeismoMatch - A computer program for spectrum matching of earthquake records", http://www.seismosoft.com/SeismoMatch-2016-Release-1.

Syrimi, P.G., Sapountzakis, E.J., Tsiatas, G.C. and Antoniadis, I.A, (2017), "*Parameter Optimization of the KDamper Concept in Seismic Isolation of Bridges Using Harmony Search Algorithm*". Proc. of the 6th International Conference on Computational Methods in Structural Dynamics and Earthquake Engineering (COMPDYN 2017), Rhodes Island, Greece, June 15-17.

Taglinski, T., Kochmann, D., Stone, D., et al. (2007), "*Composite materials with viscoelastic stiffness greater than diamond*". Science, **315**, 620–622.

Tezcan, S. S. and Civi, A. (1979), "*Reduction in Earthquake Response of Structures by means of Vibration Isolators*", U.S. National Conference on Earthquake Engineering, Stanford University, Stanford, California.

Tezcan, S. S., Civi, A. and Huffman, G. (1980), "*Advantages of Spring-Dashpot Systems as Vibration Isolators*", Report No. 80-31E, Earthquake Engineering Research Institute, Bogazici University.

Tezcan, S. S. (1982), "*The Use of Seismic Isolation Techniques in Design*", Report No. 82-41E, Earthquake Engineering Research Institute, Bogazici University.

Virgin, L., Santillan, S. and Plaut, R. (2008), "*Vibration isolation using extreme geometric nonlinearity*". Journal of Sound and Vibration, **315**, 721-731.

Virk, K., Monti, A., Trehard, T., et al. (2013), "*SILICOMB PEEK Kirigami cellular structures: mechanical response and energy dissipation through zero and negative stiffness*". Smart Materials and Structures, **22**.

Wang, X., Gao, X.Z. and Ovaska, S.J. (2009), "*Fusion of clonal selection algorithm and harmony search method in optimization of fuzzy classification systems*". International Journal of Bio-Inspired Computation, **1**, 80-88.

Weber B. and Feltrin G. (2010), "*Assessment of long-term behavior of tuned mass dampers by system identification*". Engineering Structures, **32**, 3670-82.

Winterflood, J., Blair, D. and Slagmolen, B. (2002), "*High performance vibration isolation using springs in Euler column buckling mode*". Physics Letters A, **300**, 122-130

Wright, F.L. (1977), An Autobiography: Frank Lloyd Wright. Horizon Press, New York.

Zhou, J., Xu, D. and Bishop, S. (2015), "*A torsion quasi-zero stiffness vibration isolator*". Journal of Sound and Vibration, **338**, 121–133.

Zhou, N. and Liu, K. (2010), "*A tunable high-static–low-dynamic stiffness vibration isolator*". Journal of Sound and Vibration, **329**, 1254–1273.